Final Report
National Aeronautics and Space Administration
Lewis Research Center
Grant NGR 23-004-068

RESEARCH ON FREE AND IMPINGING JETS FOR THE DEVELOPMENT OF STOL AIRCRAFT

Division of Engineering Research
MICHIGAN STATE UNIVERSITY
East Lansing, Michigan 48824
January 21, 1974

Final Report
National Aeronautics and Space Administration
Lewis Research Center
Grant NGR 23-004-068

RESEARCH ON FREE AND IMPINGING JETS FOR THE DEVELOPMENT OF STOL AIRCRAFT

Prepared by

John F. Foss
Stanley J. Kleis

Division of Engineering Research
MICHIGAN STATE UNIVERSITY
East Lansing, Michigan 48824
January 21, 1974

1. INTRODUCTION

Research on the behavior of jets, related to externally-blown-flap (e.b.f.) configuration for STOL aircraft, has been conducted at Michigan State University for a three-year period under a continuing grant from NASA Lewis Research Center NGR 23-004-068. This final report for the project will summarize the nature and principal results of the total research activity, identify the major contributions of the program which support the technical mission of NASA, and identify the further research efforts which are suggested by the work reported herein and the NASA mission.

2. THE RESEARCH PROGRAM

2.1. Shallow Angle Oblique Jet Impingement

2.1.1. Documentation and aerodynamic considerations

The original problem under investigation was a shallow angle, $0 \leq \alpha \leq 15$ degrees, jet impingement flow to simulate the fan jet exhaust-main airfoil interaction (see Figure B-1*). Flow visualization studies were first conducted to identify the gross characteristics of the flow field. Simultaneously, computer programs were developed for the acquisition of quantitative data. The flow visualization studies revealed that the flow maintained a relatively narrow structure (see Figure 1) and that sampling the surface pressures and velocities at constant values of the longitudinal distance from the nozzle would be appropriate. The data was acquired within the spatial domain $0 \leq x/d \leq 6$ and for h/d values of $0.5 \leq h/d \leq 2$ of the shallow impingement flow; these conditions were prescribed by the e.b.f. application problem. A large quantity of mean velocity and turbulence insensity data was collected at integer x/d locations for this three-dimensional flow field. Surface pressure data for the same geometric conditions, but at more frequent intervals in the streamwise direction, were also acquired. This data was initially processed and presented to provide information pertinent to the aerodynamic characteristics of the flow. These results are presented in the First Annual Report, Foss and Kleis (1971).

A factor of major concern in the preparation of this report was the construction of suitable measures of the flow characteristics to condense the large data base into a form which could be interpreted and which would allow comparisons of the various geometric conditions. The data from the

*Figures numbered B-_ refer to Appendix B.

numerous velocity traverses was effectively summarized in terms of isotachs (contours of constant mean flow speed); a sample set of isotachs is shown in Figure B-6. Similarly, the surface pressure data was presented in the form of isobaric contours; these suggest a footprint-like pattern (see Figures B-2, B-4, B-5). (Strikingly, the zero isobar had an identical shape as that of the surface oil pattern in the flow visualization studies.)

2.1.2. The governing mechanics and acoustic considerations

Essentially the same data base was used to establish the governing mechanics for the shallow angle impingement flow. These considerations are completely reported in the Second Annual Report (see Foss and Kleis, 1972). The presence of the plane surface in the jet path requires the jet to spread laterally, deflect vertically, or execute a motion which is some combination of these. It has been shown that the jet response is essentially a vertical deflection for a small impingement angle. The mechanistic reasons for this are presented in the report. Essentially, a balance of the pressure force and the vertical momentum flux component is achieved with such a sufficiently small lateral pressure gradient that the lateral motion remains a small fraction of the forward speed. Also, the detailed behavior of the isotachs and isobars have been explained in terms of the vorticity transport equation. The separate processes of vorticity production by stretching and reorientation and the flux of vorticity through the plane of the impact plate (a result of the surface pressure gradients) are shown to yield the characteristic isotach contours (see Figure B-6). The formulation of this flow model from the pressure and velocity data and from the analytical considerations of the equations of motion is a major result of the total study. The flow model allows a basis for interpolation and a limited extrapolation of the results and provides the basis for recognizing the increased complexity of the large angle impingement flows. The mechanics of the shallow angle impingement case was the subject of a technical abstract presented at the Fourth Canadian Congress of Applied Mechanics by Foss and Kleis (1973). This abstract is reproduced as Appendix A since it succinctly summarizes this aspect of the total research program.

The vorticity considerations, which are essential to a description of the mechanics of the oblique jet impingement flow field, can also be employed in an attempt to identify the mechanistic factors responsible for

the generation of acoustic noise. Using the analytical developments of Powell (1964), the far field acoustic intensity can be related to the second time derivative of the circulation about a vortex loop. Two characteristics of the flow are of central importance in relationship to this acoustic source effect. First, the introduction of vorticity into the flow resulting from the surface pressure gradients and the consequent restructuring of vortex loops in the turbulent motion contribute to a strong time dependence of the circulation about the loops. Secondly, the presence of the stagnation streamline in the low velocity shear layer below the jet centerline requires a strong and rapid restructuring of the approaching axisymmetric vortex loops in the neighborhood of and/or below the stagnation streamline. Since these vorticity-acoustic considerations do not appear in any of the reports filed in conjunction with this grant, a copy of a symposium paper, Foss (1973), is included in this report as Appendix B.

2.2. Large Angle Oblique Jet Impingement

In recognition of the e.b.f. application and as a logical extension of the earlier investigation, a study of the large angle oblique jet impingement flow field was conducted during the third year of the grant. An entirely new flow system with a new probe traverse and position control system and a new computer-based data acquisition capability were developed for this study. The new physical equipment was necessitated by the large angle and consequent "radial character" of the flow field. The new computer routines were necessitated by the strong three-dimensional character of the flow. Figures 2 and 3 are schematic representations of the new physical facilities, and Figure 4 indicates the coordinate system adopted for the description of this flow. The details of the experimental facility and a presentation and discussion of the results (acquired to date) to document the flow field of a large angle impingement condition are described in a technical report, Foss (1974). Characteristic results showing the surface pressure field and the centerplane velocity and turbulence intensity fields are presented in Figures 5 and 6. (The three-dimensional velocity field characteristics are presented in the technical report.) These results will also be presented at the Second Interagency Symposium on University Research in Transportation Noise. The abstract for this presentation is included as Appendix C.

2.3. The Effect of the Exit Plane Conditions on the Near Field of An Axisymmetric Jet

Laboratory investigations of the fundamental characteristics of jets have, in general, been executed with a quiescent core flow. This is a scientifically reasonable approach; it establishes the behavior of jets with a minimum number of complicating features. However, from a technological standpoint, many jets of interest are characterized as having some combination of mean velocity gradients and turbulence structure at the exit plane. The turbulence structure in the noise producing region of a free jet, the performance of a jet exhaustor, and the structure of the jet (and hence the noise producing characteristics) as it approaches the impingement region of an e.b.f. are examples of technologically important flows which are influenced by the exit plane conditions. From a fundamental standpoint, the jet flow constitutes a solution to a boundary value problem. Such a solution is not only a function of the Mach and Reynolds numbers (for a submerged flow), but also of the boundary conditions; i.e., the mean velocity and turbulence structure at the exit plane. These considerations in general, and an indication that the near field mass flux was dependent upon the exit plane conditions in particular, were the motivation for a major investigation of the exit plane flow structure effects in jet flows. A special configuration was developed to allow an independent control of the scale and intensity of the turbulence at the exit plane of the jet, and exhaustive measurements were made in the region $0 \leq x/d \leq 10$ for eight distinct exit plane conditions. The detailed motivation, experimental procedures, and results of this investigation are fully reported by Kleis and Foss (1974). The technique for creating the various exit plane conditions is shown in Figure 7, and three characteristic homogeneous turbulence field conditions (the mean velocity profile was uniform) are presented in Figure 8. The major results of this study may be summarized as: 1) the momentum flux in the near field ($0 \leq x/d \leq 10$) is not constant; it increases to approximately 125 percent of its original value (the static pressure within the jet field must decrease accordingly to allow for this acceleration of the flow); 2) this behavior and the streamwise dependence of the mass flux are "independent" of the turbulence structure at the exit plane of the jet; 3) the exit plane effects are manifest in the turbulence structure of the near field jet, and these results contribute to the

development of a mechanistic description of the orderly structures in jet turbulence identified and discussed by Crow and Champagne (1971). The turbulence field characteristics of this flow will also be presented at the Second Interagency Symposium on University Research in Transportation Noise. The abstract for this paper is included as Appendix D.

3. CONTINUING AND FUTURE RESEARCH

3.1. Large Angle Oblique Jet Impingement*

The large angle oblique jet impingement three-dimensional flow field will be documented in terms of 1) mean velocity, 2) Reynolds stress, and 3) appropriate correlation function measurements. Using these measurements in the analytical formulations derived for the shallow angle impingement flow and by developing additional analytical considerations as appropriate, the governing mechanics of this flow will be examined. Selected measurements for other angles and additional analytical relationships may be necessary for the development of a complete flow model.

An elaborate scheme to measure the instantaneous vorticity transverse to the mean streaming flow direction and parallel to the plate will be used to document the vorticity characteristics of the flow. These measurements are of considerable interest in terms of their relationship to the generation of acoustic noise.

Since the measurement of "point wise" vorticity values is not common, special note will be made herein of the proposed technique. The vorticity component to be measured is Ω_t which is defined in the intrinsic coordinates of the mean flow field (see Figure 4). In terms of the velocity, this vorticity component is

$$\Omega_t = \frac{\partial u_s}{\partial z} - \frac{\partial w}{\partial s} . \qquad (1)$$

(Note: The use of the lower case symbol for a fluctuating quantity is suspended for this discussion; u_s, etc., are instantaneous quantities.) The quantity $\partial w/\partial s$ will be measured by invoking an instantaneous "frozen turbulence" assumption from which $\partial w/\partial s$ may be inferred, specifically

$$\frac{\partial w}{\partial s} = - u_s^{-1} \frac{\partial w}{\partial t} . \qquad (2)$$

*The investigation discussed in this subsection is being supported by the Noise Control Section at NASA Langley Research Center, Dr. Jay Hardin, Grant Monitor.

An analog differentiating circuit will be used to form $\partial w/\partial t$; the subsequent processing will be digital. The simultaneous measurement of $\partial u_s/\partial z$ at the same point is not possible; however, it is possible to take advantage of the spanwise orientation of the desired quantity (i.e., Ω_t) and to approximate $\partial u/\partial z$ as

$$\frac{\partial u}{\partial z} \cong \frac{u(z + \Delta z) - u(z)}{\Delta z} = \frac{\Delta u}{\Delta z} \tag{3}$$

where two horizontal wires can be mounted next to the x-array and displaced in z at a distance approximately that of the x-wire vertical span. The difference between the two wires will be formed digitally. This measurement is subject to the error sources of the approximation in (3) and because of the necessity to form w(t) from analog signal processing. There is an additional error in that the single wires respond to w as well as u; hence the difference in the two voltage signals is

$$\begin{aligned} \Delta e &= \Delta(u_s^2 + w^2)^{1/2} \\ &= \Delta u_s[1 + (w/u_s)^2]^{1/2} \\ &\cong \Delta u_s + \frac{1}{2}\Delta (w/u_s)^2 + \ldots . \end{aligned} \tag{4}$$

Near the plate, $w/u_s \lesssim 0.2$; hence, this error source is not significant in the region where the Ω_t measurements are of most interest.

The measurement of the transverse vorticity will allow several of its important statistical measures to be evaluated. Specifically,

$$\overline{\Omega}_t, \quad \overline{\omega_t^2}, \quad \overline{\omega_t(t)\omega_t(t+\tau)} \tag{5}$$

will be determined for the regions which are presumed most responsible for the acoustic noise generation.

3.2. Effect of the Exit Plane Conditions on the Development of An Axisymmetric Jet

A logical extension of the present study is the inclusion of a mean velocity gradient at the exit plane of the jet in addition to the turbulence structure in the jet core. The extensive data acquisition programs and experimental methods developed for the just-completed study can be immediately utilized for the new study. Several techniques for the control of the exit plane conditions are feasible, including an axisymmetric and

variable length, $\ell = \ell(r)$, honeycomb or a boundary layer thickening technique* in conjunction with the free stream turbulence generator previously used. The latter approach has the advantage that the relationship to previous results is more apparent. The former scheme has the advantage that a controllable and wider range of mean velocity gradients will be available.

3.3. Jet Studies

The experimental facility which has been developed in conjunction with the investigations described herein constitutes a valuable resource for jet studies in general. The computer controlled data acquisition system, which includes stepping motor positioning of the probe's position and orientation, allows a large volume of data to be generated with relative ease. In addition, the digitized calibration and signal processing routines with the "automatic" retention of the most significant bits (see Kleis and Foss, 1974) ensures an uncommonly high accuracy of the data. Of particular significance is the conditional sampling routine which makes use of the x-wire output to orient the hot-wire probe into the time average flow direction of the vortical and, separately, the nonvortical fluid stream at a given longitudinal-radial position. Since the hot-wire probe is calibrated in the streaming flow direction and since there can be as much as 130 degrees(!) between the mean streaming flow directions of the vortical and nonvortical fluid, the accuracy of the data generated from this application of conditional sampling is significantly improved over that of standard techniques.

This data acquisition and storage capability is of particular importance in terms of evaluating turbulent flow calculation techniques. As discussed extensively by the evaluation committees of the Free Turbulent Shear Flows Conference (see Birch et al., 1973), there is a significant need for accurate and fully documented data to be used as a test case for the approximate (but tractable) schemes to calculate turbulent shear flows. The capability to generate and document data in a form which may be readily interpreted by a digital computer (e.g., cards, magnetic or paper

*If a series of jets are directed upstream and at a shallow angle into the boundary layer plate, a large turbulent boundary layer can be developed in a short distance. This technique was developed at I.I.T., see Morkovin, et al. (1972).

tape, etc.) is considered to be a significant by-product of the research support provided by this grant.

4. REFERENCES

1. Birch, S. F., D. H. Rudy, and D. M. Bushnell (editors), "Free turbulent shear flows," Vol. I, NASA SP-321 (1973).
2. Crow, S. C., and F. H. Champagne, "Orderly structure in jet turbulence," Jour. Fluid Mech., Vol. 48 (August 1971).
3. Foss, J. F., and S. J. Kleis, "A study of the round-jet/plane-wall flow fluid," First Annual Report, Grant NGR 23-004-068 (October 1971).
4. Foss, J. F., and S. J. Kleis, "The oblique impingement of an axisymmetrical jet," Second Annual Report, Grant NGR 23-004-068 (December 1972).
5. Foss, J. F., "Vorticity effects in oblique jet impingement flows as background for the acoustics problem," Interagency Symposium on University Research in Transportation Noise, edited by G. Banerian and K. Karamcheti, Vol. I, 273, Stanford University (March 1973).
6. Foss, J. F., and S. J. Kleis, "The oblique impingement of an axisymmetric jet," Proc. Fourth Canadian Congress of Applied Mechanics, Montreal (May 1973).
7. Foss, J. F., "Measurements of a large angle oblique jet impingement flow," Third Year Technical Report, Grant NGR 23-004-068, to be issued (1974).
8. Kleis, S. J., and J. F. Foss, "The effects of exit conditions on the development of an axisymmetric turbulent free jet," Third Year Technical Report, Grant NGR 23-004-068, to be issued (1974).
9. Morkovin, M. V., H. M. Nagib, and J. T. Yung, "On modeling of atmospheric surface layers by the counter-jets technique, preliminary results," I. I. T. Themis Tech. Report R 72-7 (October 1972).
10. Powell, A., "Theory of vortex sound," Jour. of the Acoustical Soc. of America, Vol. 36, part 1, 177-195 (January 1964).

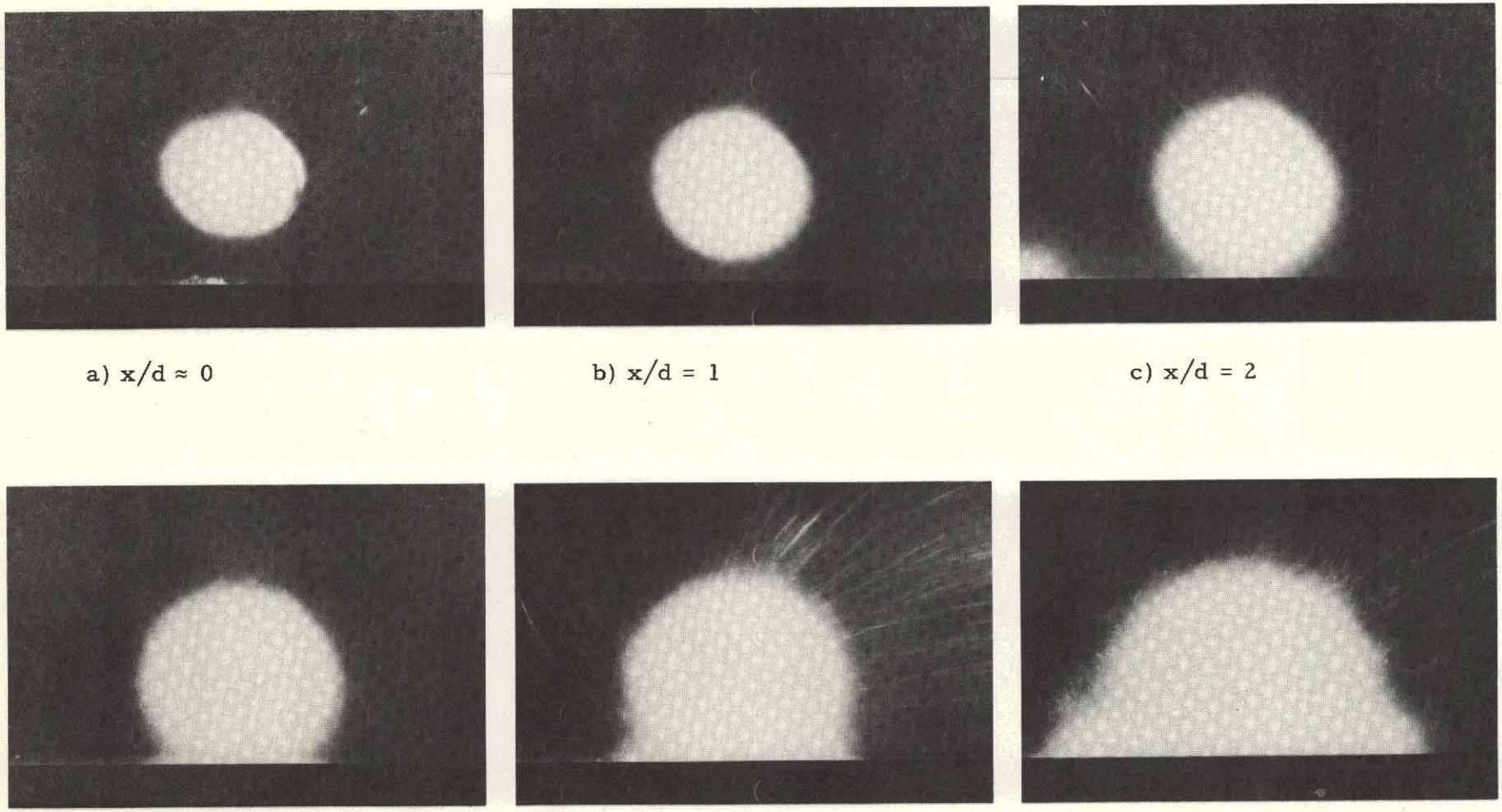

a) x/d ≈ 0 b) x/d = 1 c) x/d = 2

d) x/d = 3 e) x/d = 4 f) x/d = 5

Figure 1. The cross section of a powder seeded jet (as shown by a plane sheet of light) to demonstrate the existence of streamwise vorticity. α = 6 degrees, h/d = 0.75.

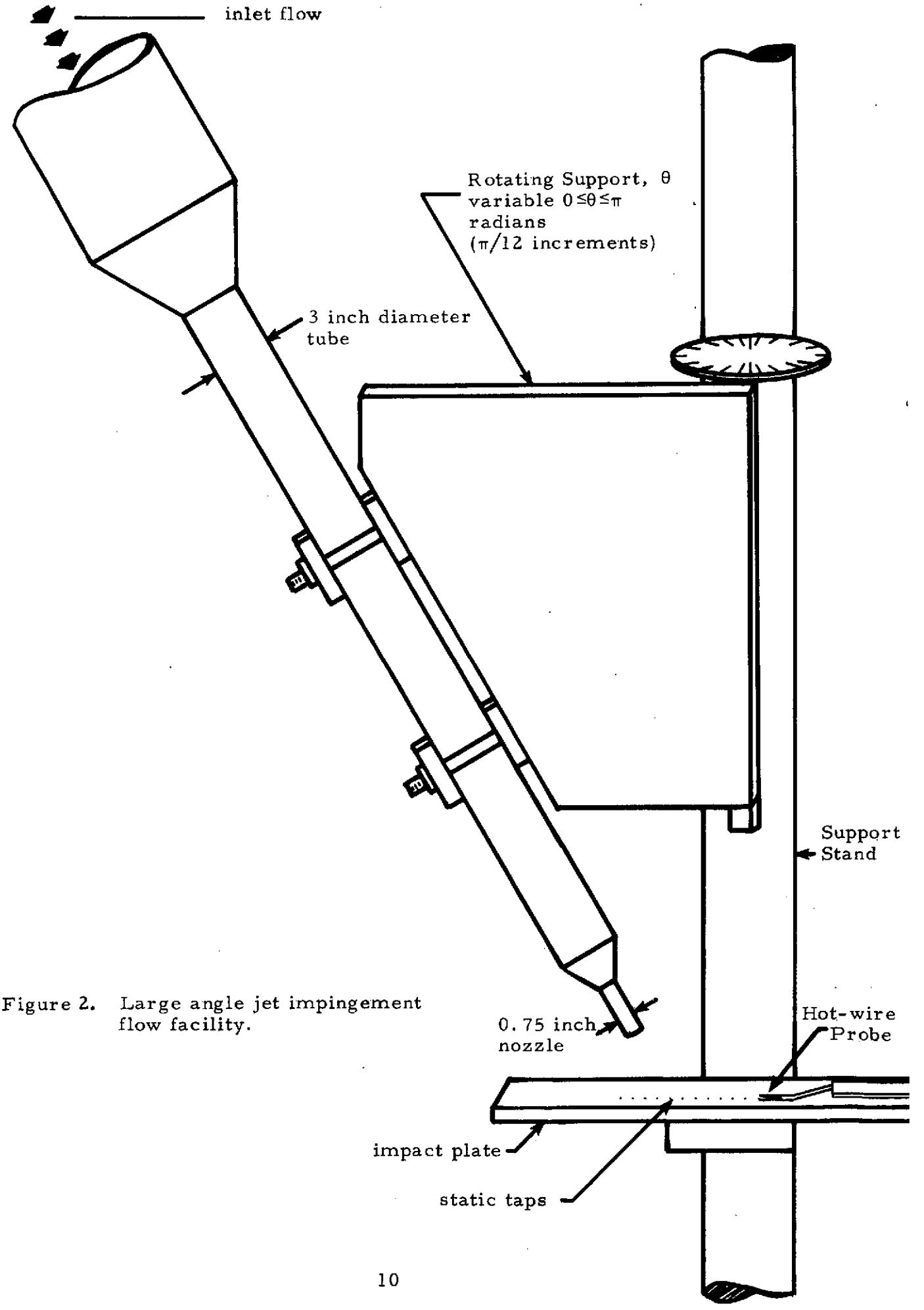

Figure 2. Large angle jet impingement flow facility.

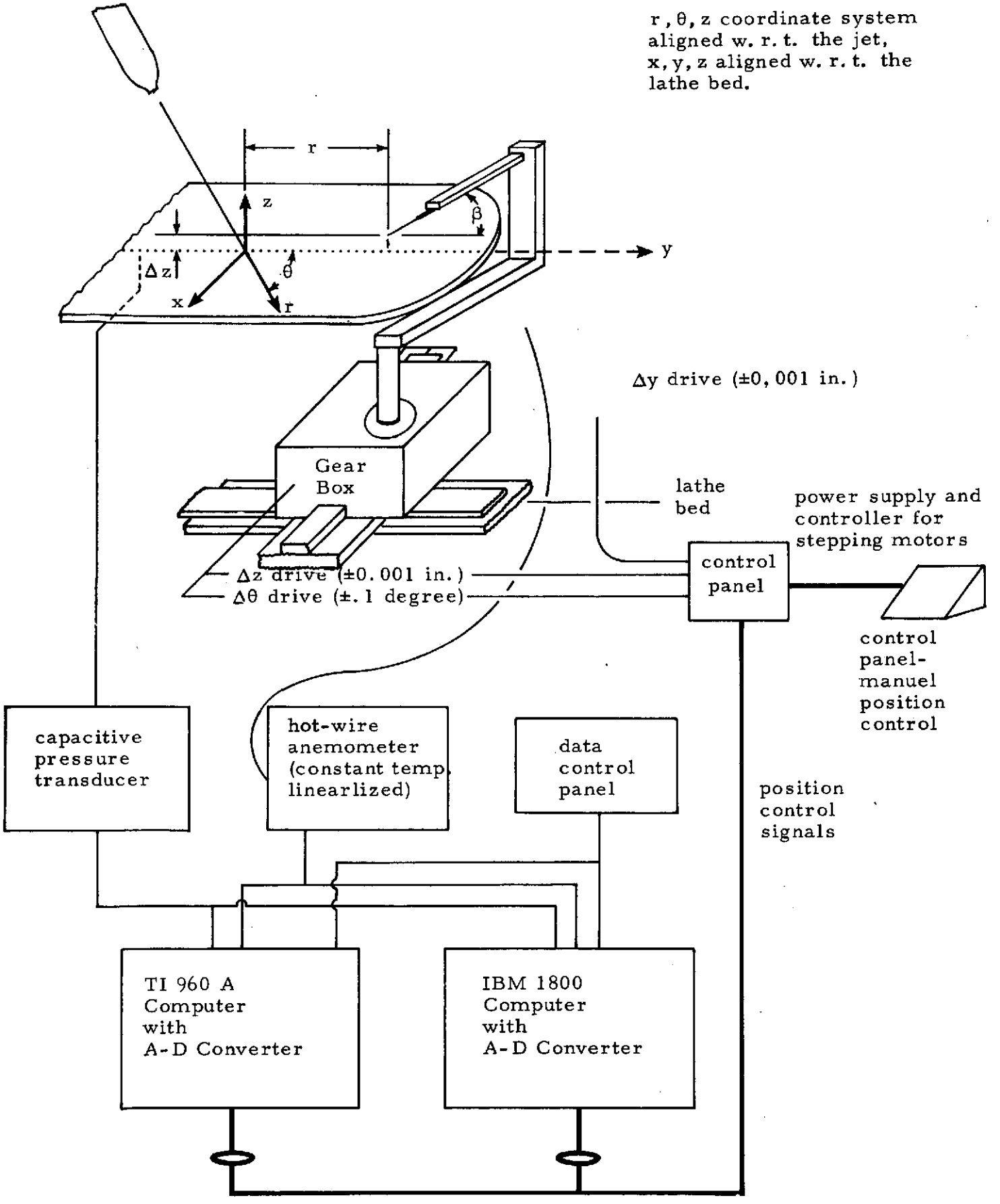

Figure 3. Schematic of data acquisition facility.

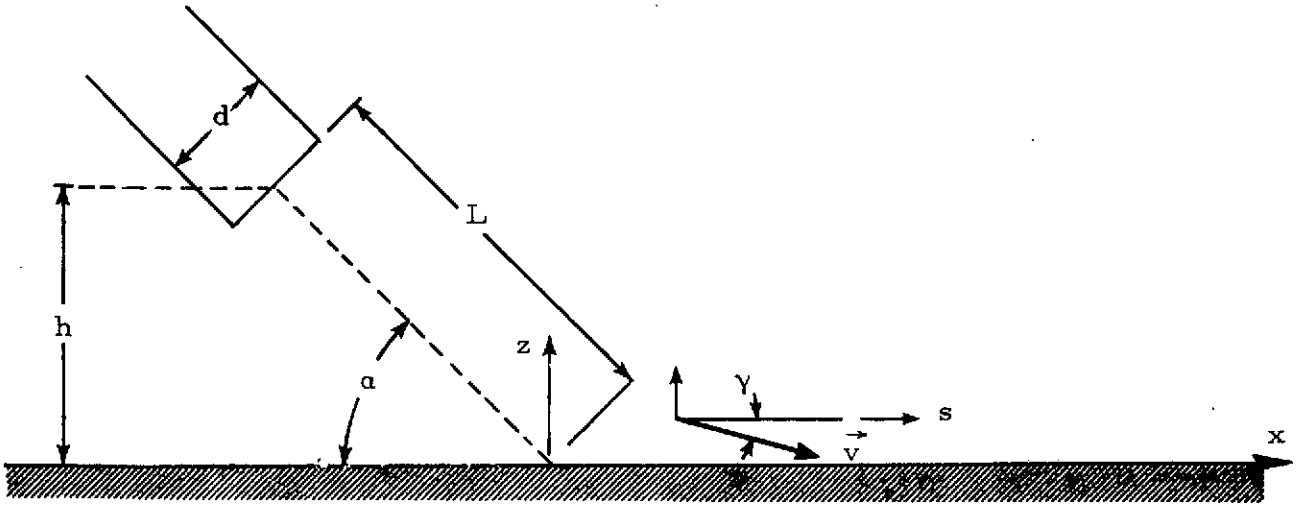

a. Side View

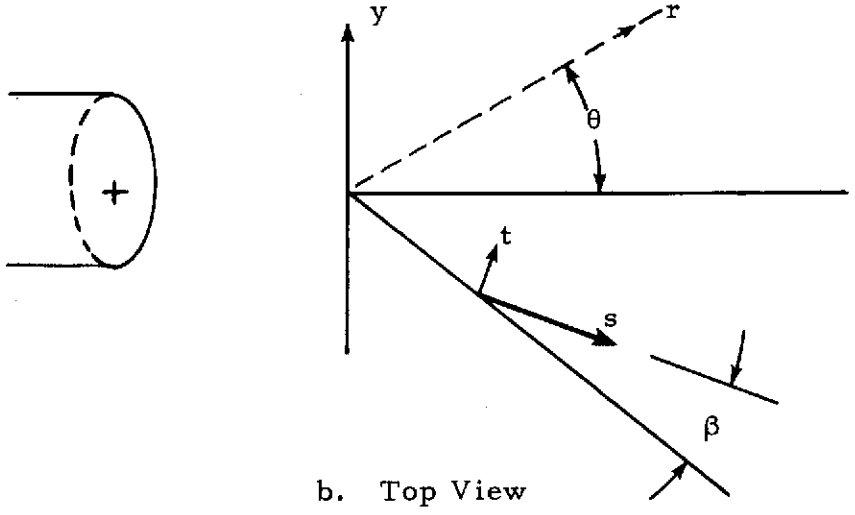

b. Top View

Figure 4. Coordinate system and definition of symbols for the large angle jet impingement studies.

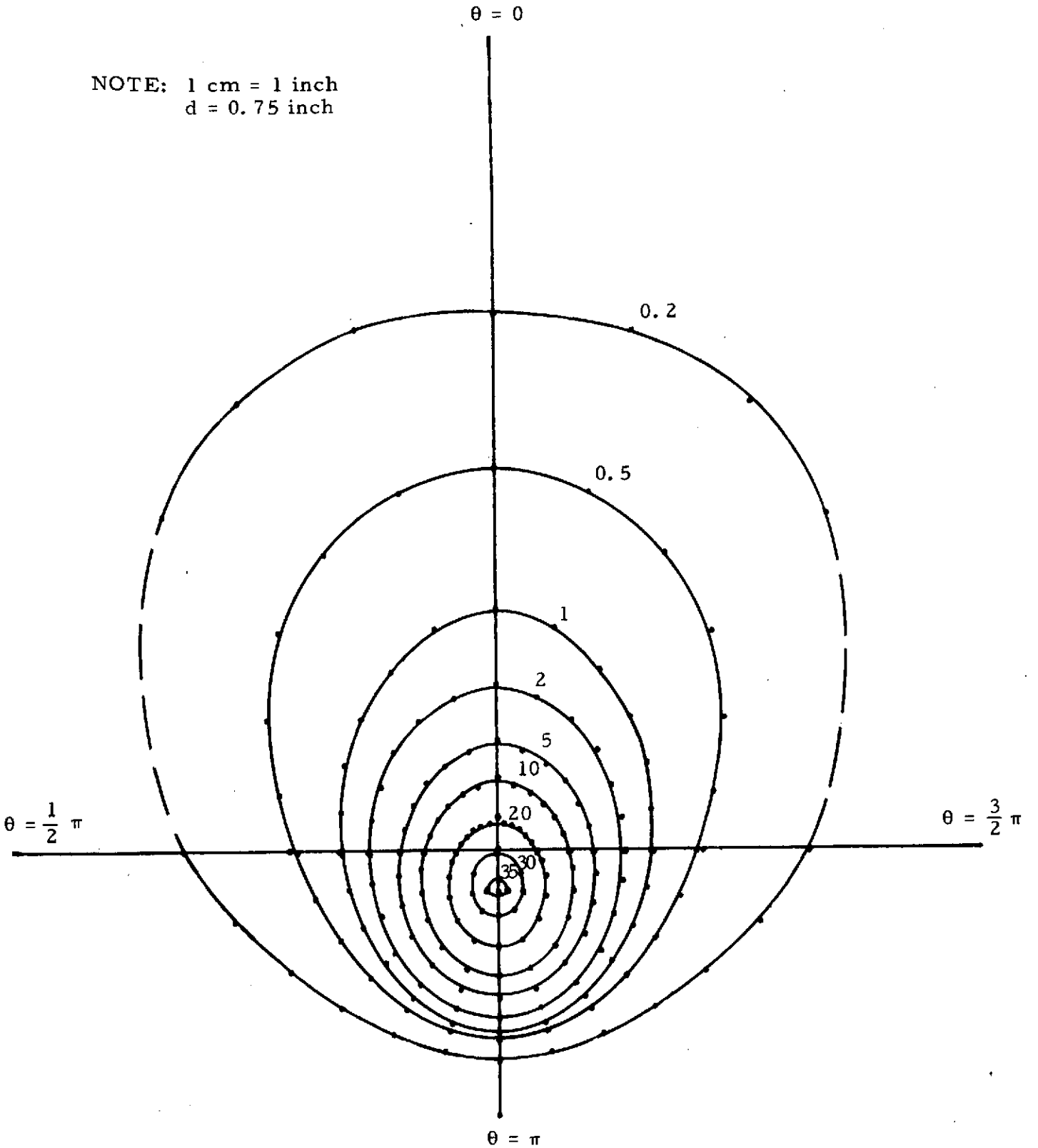

(a) Complete data set

Figure 5a. Surface pressure isobar contours. α = 45 degrees, L/d = 7, jet Reynolds number = 4.8×10^4.

Contours represent level curves of $100 \dfrac{(p - p_{atm})}{\rho u_o^2 \lambda \sin \alpha}$

$\lambda = \int_{A_{jet}} \rho u^2 dA / \rho u_p^2 A_{jet}$, λ = 0.809 taken from [5].

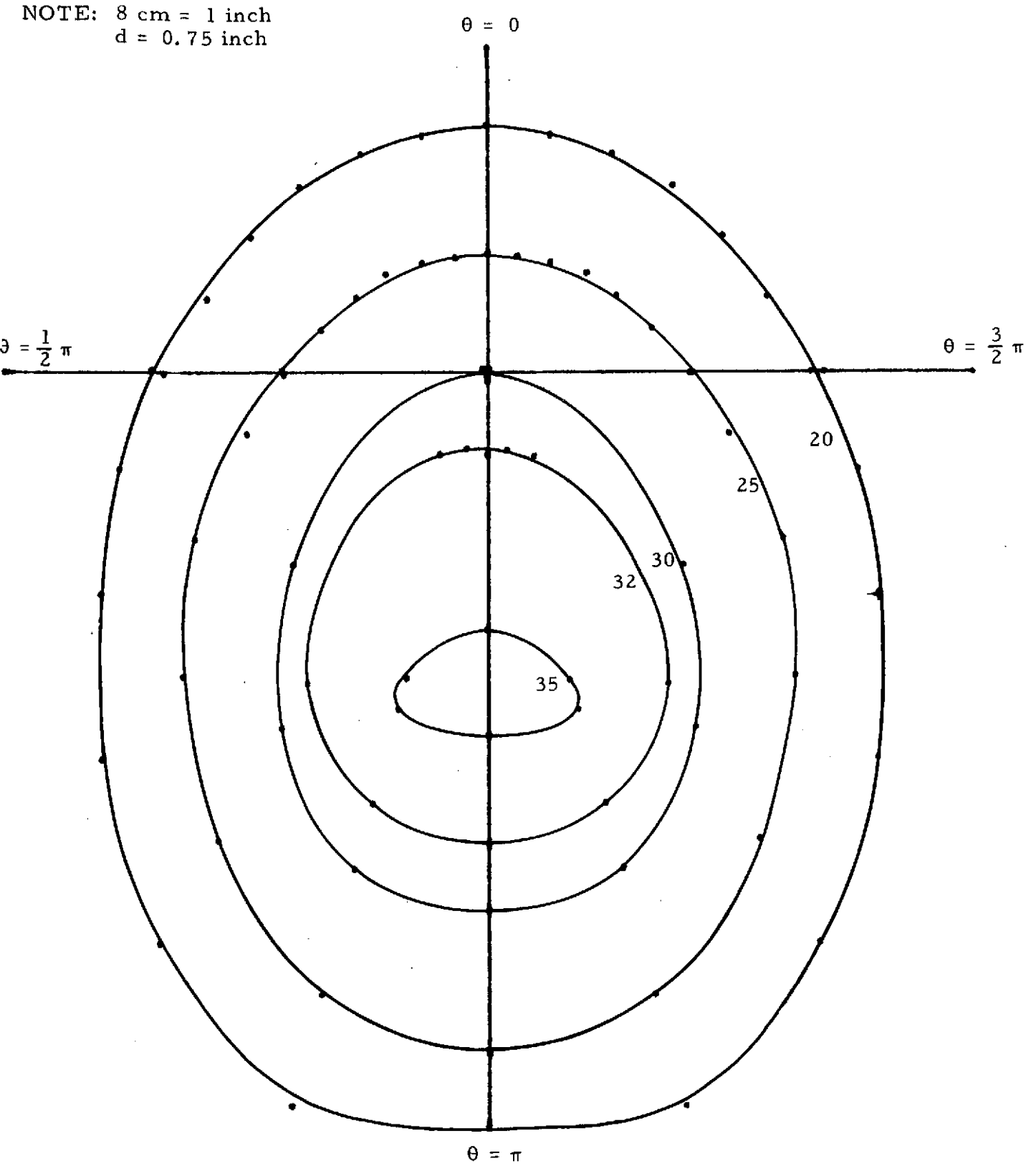

Figure 5b. Expanded scale to show detail of the maximum pressure region.

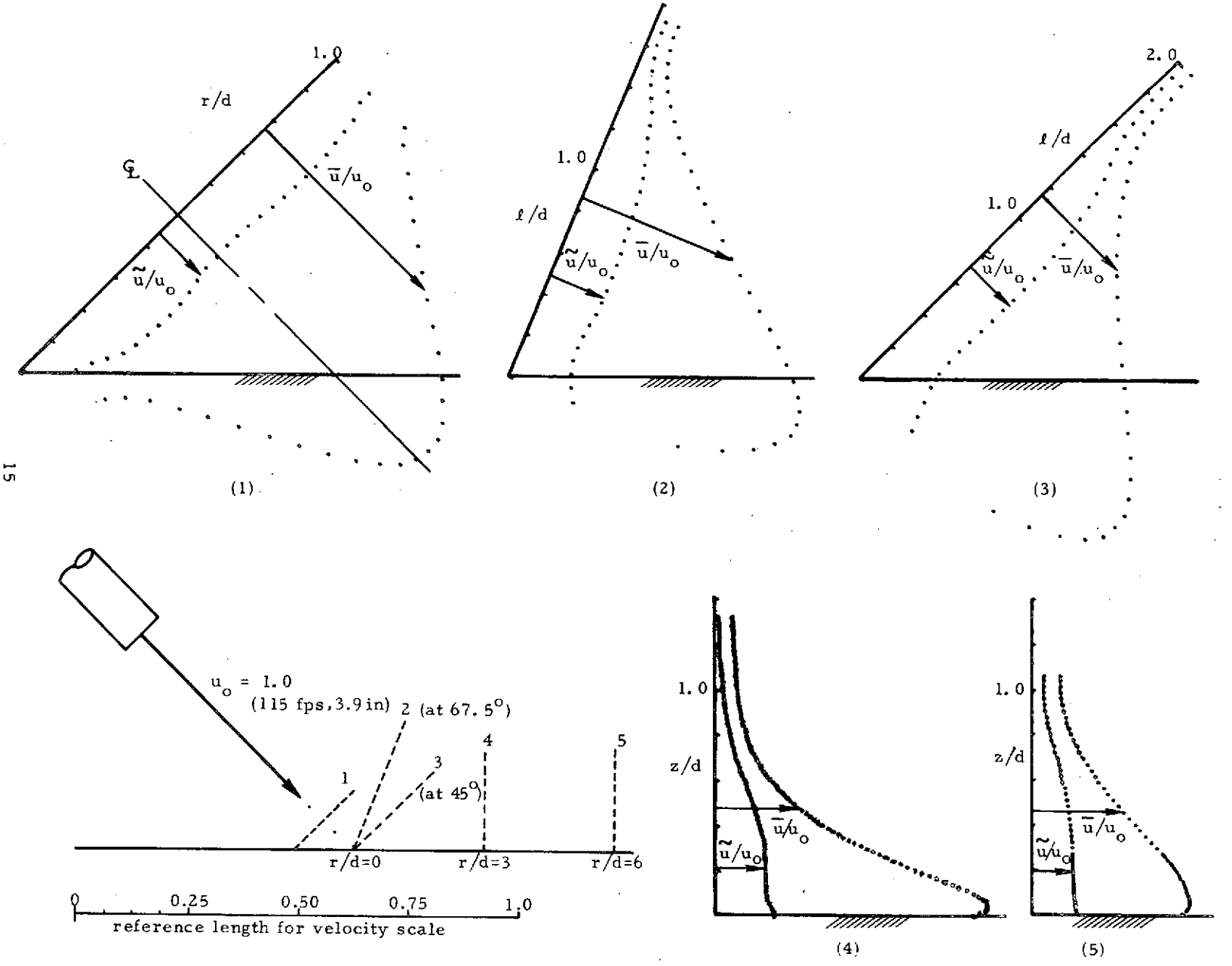

Figure 6. Velocity magnitude traverses in the $\theta = 0$, $\theta = \pi$ plane.

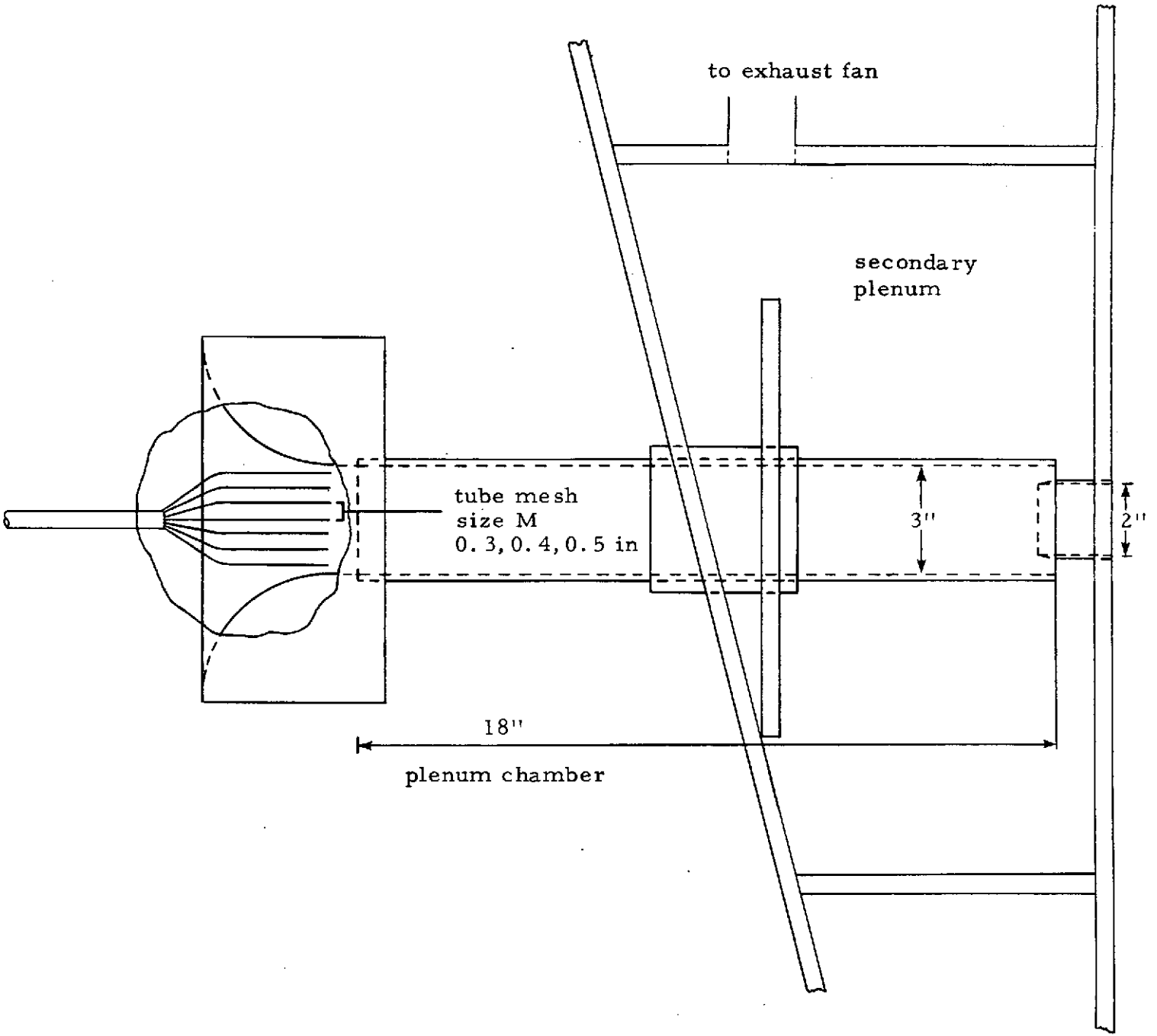

Figure 7. Configuration to achieve controlled intensity and scale at exit plane of axisymmetric jet.

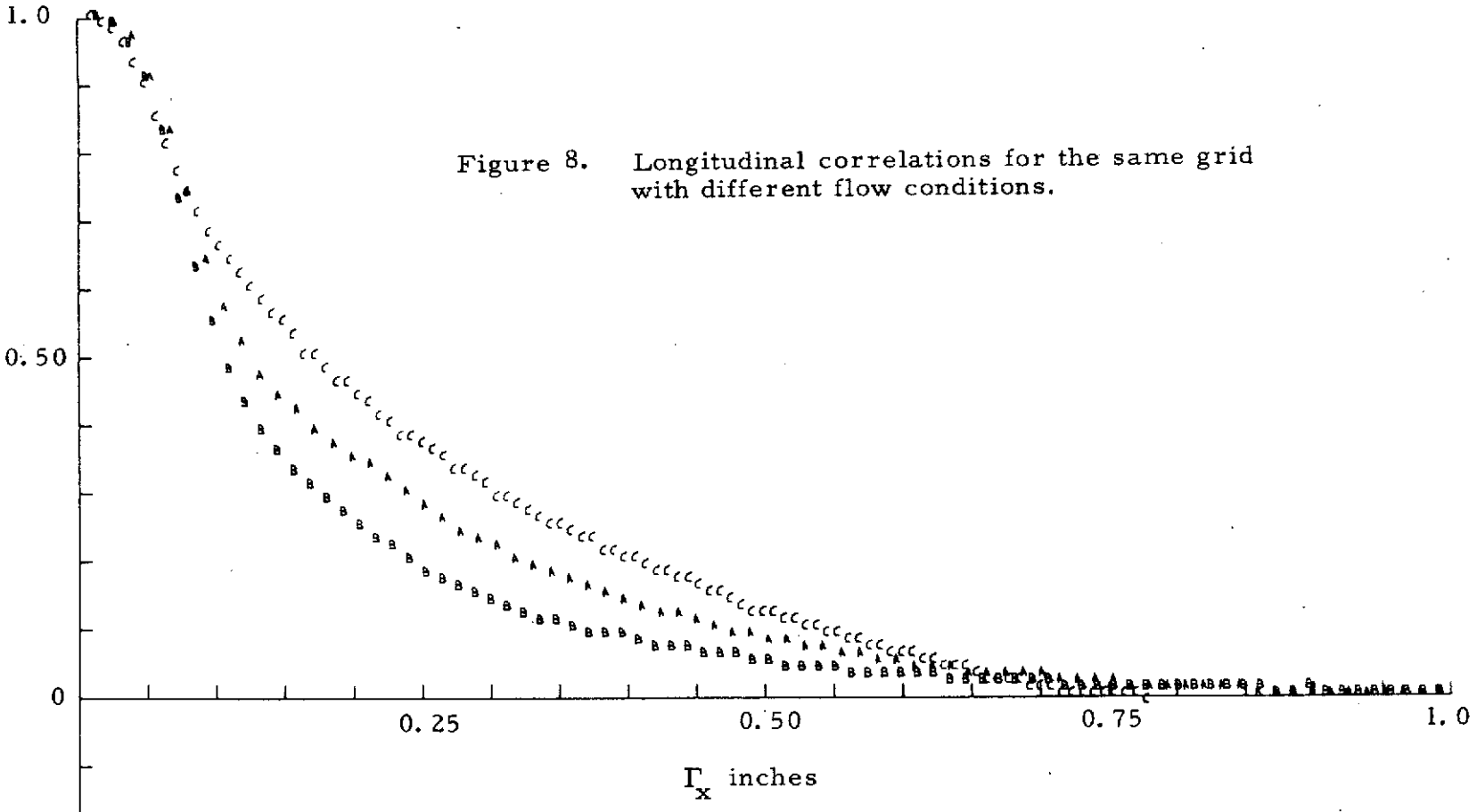

Figure 8. Longitudinal correlations for the same grid with different flow conditions.

Legend:

	M	supply pressure	blower RPM	U ± tolerance (fps)	$\tilde{u}$ ± tolerance (percent)
A	0.5	15	980	111.2 ± 1.5	2.4 ± 0.3
B	0.5	5	980	99.5 ± 0.5	1.25 ± 0.2
C	0.05	20	0	65.1 ± 0.7	2.8 ± 0.3

APPENDIX A

THE OBLIQUE IMPINGEMENT OF AN AXISYMMETRIC JET

John F. Foss
Associate Professor
Dept. of Mech. Engr.
Michigan State Univ.
East Lansing, Mi. 48823

Stanley J. Kleis
Graduate Research Asst.
Division of Engr. Res.
Michigan State Univ.
East Lansing, Mi. 48823

The oblique impingement of an axisymmetric jet on a plane wall, see Figure 1, has been investigated. The important kinematic and dynamic characteristics of the mean flow jet/plate interaction have been identified for shallow angle ($\alpha \lesssim 12$ degrees) cases. This study was motivated by the externally blown flap configuration for STOL aircraft. A streamwise domain of $0 \leq x/d \leq 5$ is of interest for the application problem and was accepted as a bound for the present study. A no-penetration (kinematic), condition is imposed on the jet flow by the presence of the plate. The response of the jet to this constraint is a combination of upward deflection or jet curvature and lateral spreading along the surface of the plate. Dynamic phenomena govern this response. These are made evident by appropriate measures defined from the data base of mean velocity traverses u(y) at various z and integer x/d values ($0 \leq x/d \leq 5$) and surface static pressure traverses p(y) taken at discrete x locations.

Isotach contours, defined from the mean velocity measurements, indicate that the upper portion of the jet retains its axisymmetric character and that the primary isotach deformation occurs in the low velocity fluid near the plate. This general condition is restricted to sufficiently small angles (α) and large heights (h/d) such that the interaction is sufficiently weak; Figure 2 presents a typical case. This localized influence is mechanistically attributed to inertia and transverse shear ($\overline{-\rho u_x u_o}$) effects which resist the distortion of the jet.

The 0.1 isotach of the free jet can be quite well approximated by a cone; the intersection of a cone with an imaginary plate defines a reference contour. The contour defining the dynamically important jet width corresponds to the zero isobar, see Figure 3. These two contours have been compared for a large range of cases $3 \leq \alpha \leq 60$ (degrees) and $0.5 \leq h/d \leq 2$. A weak impingement condition is implied by the similar shapes and the independence of the relative widths (free isotach ≈ 0.7 zero isobar) with respect to α and h/d.

This independence implies a strong dependence of jet curvature K on these parameters. The curvature of the jet can be accurately determined using the surface pressure distribution. Two K and p(x,0,0) distributions are shown in Figure 4. An assessment of all such data indicates that the curvature is strongly dependent upon α and h/d and that the comparison of K and p(x,0,0) demonstrates the relative strength of the interaction.

The deformed isotachs can be described in terms of the streamwise vorticity field near the plate surface. The flux of ω_x at $z = 0$ is $\int_0^x p(x,0,0)/\rho \, dx$; hence the centerline pressure distribution is important in the determination of the net ω_x and the dependence of $p(x,0,0)$ on the geometric parameters, noted above, is seen to be an important characteristic of the problem. The large scale and gradual deformation of the isotach patterns demonstrated in Figure 2 can be ascribed to ω_x of the opposite sign as compared with that introduced by the surface pressure gradient (ω_σ $\partial u/\partial\sigma$ creates $\omega_x > 0$ for $y > 0$).

The stagnation point does not occur at the location of the maximum surface pressure for the oblique impingement problem. This result is demonstrated in Figure 5 which presents a comparison of v_w and v_p (equivalent velocities in the plane of the plate). The tangent point (or points) of these two curves is the stagnation point. Analytical considerations show that the limiting orientation of the stagnation streamline is

$$\lim_{\delta z \to 0 \;\; \delta x \to 0} \frac{\delta_z}{\delta_x} = \frac{-\partial\omega_x/\partial x}{(1/\mu)\partial p/\partial x}$$

where δz and δx are displacements from the stagnation point. The above analytical result is restricted to analytic u and w functions and would be invalid if a finite stagnation line existed.

This research was supported by NASA Grant NGR 23-004-068.

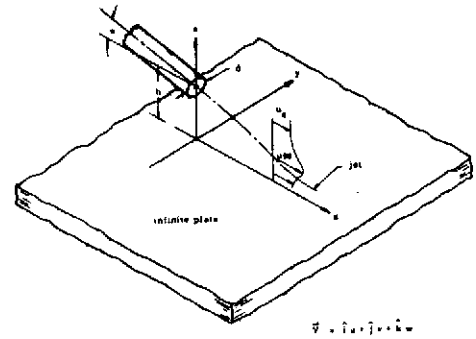

Figure 1. The oblique jet impingement flow field, coordinate system and nomenclature.

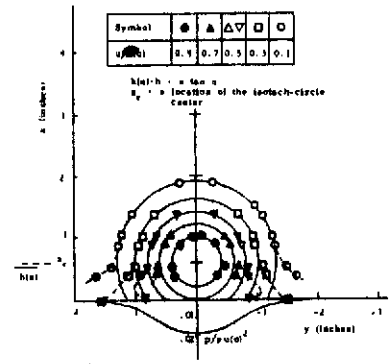

Figure 2. Isotach and pressure distribution for $\alpha = 9$, $h/d = 1$, $x/d = 4$.

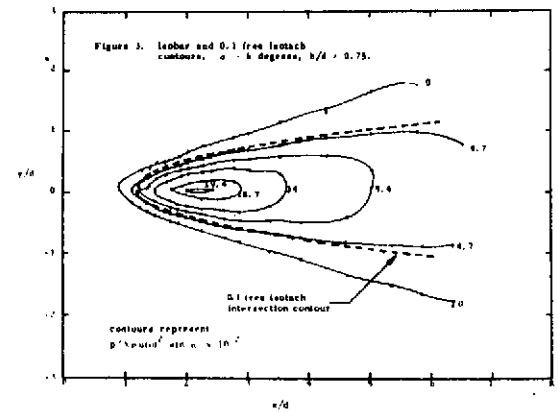

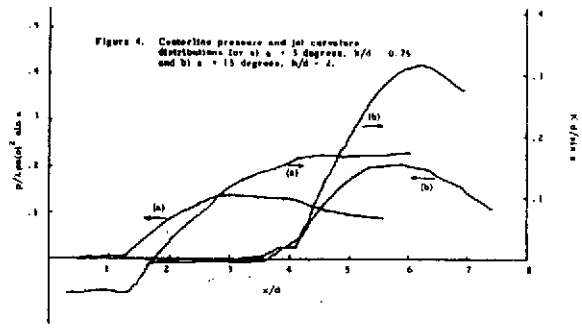

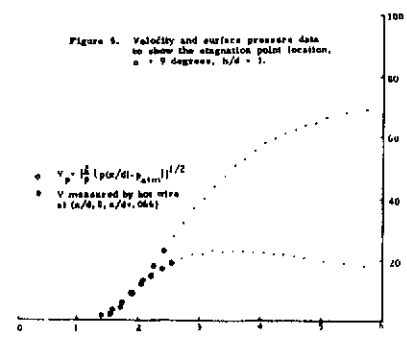

APPENDIX B

VORTICITY EFFECTS IN OBLIQUE JET IMPINGEMENT FLOWS AS BACKGROUND FOR THE ACOUSTICS PROBLEM

ABSTRACT

The governing phenomena for the oblique impingement of an axisymmetric jet are most readily described by vorticity considerations. The data which demonstrate this are summarized herein. The proposal that the acoustic emissions from the oblique jet impingement may be most effectively accounted for by vorticity effects is tentatively proposed. Considerations of the vorticity field which are pertinent to the acoustic problem are offered.

VORTICITY EFFECTS IN OBLIQUE JET IMPINGEMENT FLOWS AS BACKGROUND FOR THE ACOUSTICS PROBLEM

by

John F. Foss

Michigan State University
East Lansing, Michigan

1. INTRODUCTION

Numerous studies have recently been made concerning the increased acoustic noise associated with the externally blown flap (e.b.f.) configuration for STOL aircraft (see, for example, Dorsch, Kreim, and Olsen [1], Putnam and Lasagna [2], and Haas [3]). Of particular relevance to the physical problem considered herein are the measurements of Olsen, Miles, and Dorsch [4] which document the sound power level for normal and oblique impingement of a jet against a board. In each of these, the investigators have made appropriate measurements of some form of the acoustic emission. See Figure 1 for a schematic of the e.b.f. and the obliquely impinging jet flow fields.

The considerations of the present communication are different from and complementary in intent to those of the above mentioned studies. The unique features of the oblique jet impingement are considered in terms of the mechanics of the mean flow field. It is well known that the acoustic energy is quite small with respect to that represented by the mean and fluctuating flow field; hence, it is possible to speak of a cause/effect relationship between the aerodynamic flow and the acoustic field. *Unfortunately, the acoustic field depends upon rather* subtle characteristics of the aerodynamic flow such as the correlation between the pressure and velocity fluctuations or the fluctuating Reynolds stresses.

The purpose of the present writing is to indicate what we have learned of the mechanics of the oblique jet impingement problem, to describe the analytical descriptions which are based upon the (inferred) dominant mechanisms, and to offer some speculations regarding the contribution of these decriptions to the identification of the acoustic emission mechanics. Our primary data source is for relatively shallow incidence angles ($\alpha \leq 15$ degrees) but this has proved quite instructive since the flow develops more slowly (spatially) than for the larger incidence angle conditions in which the same basic processes are inferred to occur. (The net effect of these processes is noticeably different for the larger angles.) The oblique jet impingement is substantially different from the normal impingement case in certain details which are considered important in their contribution to the acoustic emission. These are discussed in the final section.

The data and the detailed arguments of the next section are to demonstrate that vorticity considerations are most helpful in the

description of the oblique jet impingement. That is, such a description accounts for the observed behavior of the jet flow field and allows the (easily measured) surface pressure gradients to be interpreted as a source of vorticity. The distortions of the jet field are accounted for by the physical effects of this surface vorticity flux and the vortex stretching/reorientation effects in the jet. In agreement with the general notions presented by Lighthill [5] it is felt that this is a flow field which is made more tractable in its physical description and/or numerical modeling by the the use of vorticity considerations. A parallel but tentative thesis is proposed for the consideration of the acoustics problem. That is, it is proposed that the source for the acoustic emission might be beneficially considered to arise from the vorticity effects of the flow field. Powell [6] has developed the initial structure for such considerations and relates vortex stretching to the production of acoustic noise. As in the aerodynamics considerations, this is an alternative, not a different, formulation of the problem. Since the vorticity (ω) is derived from the velocity field ($\omega = \nabla \times v$) it contains no more (in fact, less) information than the velocity field. Insofar as it can be used to account for equivalent effects it provides equivalent information; presumably, the effects associated with the rotational part of the motion. For example, Powell [6] demonstrates the equivalence of the vortex formulation with that of the quadrupole integral. The use of the momentum and continuity equations to describe the production of acoustic noise has been both successful and extensive. For example, Curle [7] and Ffowcs Williams, and Hawkings [8] have extended the pioneering work of Lighthill [9], [10] to account for the effects of surfaces such as in this problem. The importance of vorticity for the e.b.f. flow and similar problems may provide sufficient stimulation for the theoretical work required to extend Powell's initial efforts.

2. THE PRINCIPAL MECHANICS OF THE OBLIQUE JET IMPINGEMENT PROCESS*

2.1. Qualitative Description

The presence of an impermeable plane, oriented at some angle to the axis of an approaching jet, requires an appropriate response from the jet fluid. Kinematically, the mass flux disallowed through the plane of the plate will be accommodated by 1) the lateral spreading of the jet and/or 2) the vertical deflection of the centerline of the jet. The results of the oblique jet impingement study [11] show that the primary response of the jet is a vertical deflection for impingement angles α nominally less than 12 degrees. Pregressively larger impingement angles result in pronounced increases in spreading. The data of Donaldson and Snedecker [12] and Donaldson, Snedecker, and Margolis [13] are pertinent for the larger angles; the latter paper presents turbulence stresses, fluctuating pressure intensity and the

*The material in this section is abstracted from Foss and Kleis[11].

spectra of the turbulent velocity fluctuations.

The response of the jet, in terms of the spreading and curvature effects, is based upon dynamic considerations. An appropriate analytical description could be developed from the conservation of mass and momentum equations. An alternative description is predicated on the vorticity transport equation (1) and its volume integral (2) and (5). This description is motivated by the description of the approaching jet as a flow with prescribed azimuthal (about its axis) vorticity and the experimental data which shows that this axisymmetric structure is only effected by the processes occurring near the plane. As a consequence of this decription, it is possible to identify regions of important vortex stretching (i.e., regions of acoustic generation) and regions of vorticity flux through the plane surface.

2.2. Vorticity Equations

For a barotropic condition , $\rho = \rho(p)$, the vorticity transport equation is

$$\frac{D}{Dt}\,\boldsymbol{\omega} = \boldsymbol{\omega} \cdot \nabla\, \boldsymbol{v} + \nu \nabla^2 \boldsymbol{\omega} \tag{1}$$

The volume integral of this expression along with the appropriate use of the Gauss theorem results in

$$\int_{c.s.} \overline{\boldsymbol{\omega}\, \boldsymbol{v} \cdot \hat{n}}\; dA = \int_{c.v.} \overline{\boldsymbol{\omega} \cdot \nabla \boldsymbol{v}}\; d\forall + \nu \int_{c.s.} \frac{\partial}{\partial n}\, \overline{\boldsymbol{\omega}}\; dA \tag{2}$$

where the overbar is to signify a time average. The last term in the above expression will be important in the balance of the equation only at those points where the viscous effects are important, specifically, at the surface of the plane. The momentum equation at the surface allows the pressure gradient to be related to the vorticity gradient as

($j \cdot \boldsymbol{v} = v$, $k \cdot \boldsymbol{v} = w$, and $\big|_0$ implies evaluation at $z = 0$)

$$\frac{1}{\rho}\frac{\partial p}{\partial y}\bigg|_0 = \nu \frac{\partial^2 v}{\partial z^2}\bigg|_0 = -\nu \frac{\partial}{\partial z}\, \omega_x\bigg|_0 \tag{3}$$

for the y-component since $Dv/Dt\big|_0 = 0$. A similar development for the z-component results in

$$\frac{1}{\rho}\frac{\partial p}{\partial x}\bigg|_0 = \nu \frac{\partial}{\partial z}\, \omega_y\bigg|_0 \tag{4}$$

These expressions may be used in (2) to develop the control volume form of the vorticity transport equation

$$\int_{c.s.} \overline{\underline{\omega}\,\underline{u}\cdot\hat{n}}\; dA = \int_{c.v.} \overline{\underline{\omega}\cdot\nabla\underline{u}}\; d\forall + \hat{i}\int_{A_{plane}} \frac{1}{\rho}\frac{\partial p}{\partial y}\; dA$$

$$-\hat{j}\int_{A_{plane}} \frac{1}{\rho}\frac{\partial p}{\partial x}\; dA - \hat{k}\int_{A_{plane}} \nu\frac{\partial}{\partial z}\,\omega_z\; dA \qquad (5)$$

Equation (5) shows that the efflux of vorticity from the control volume can differ from that entering by production (vortex stretching) and the flux through the surface.

2.3. Pertinent Experimental Results

A useful reference for the oblique jet impingement problem is the intersection of a free jet isotach* surface with an imaginary plane at the location of the physical plate surface. The isobar contours formed from the surface pressure measurements form a characteristic imprint of the jet impingement and a comparison of the two contours provides a relative measure of the spreading. The data of the α = 9 degrees, h/d = 1 case has been selected from [11] to demonstrate the relatively constant width ratio between the two contours. The complete data are summarized in Table 1. From these data, it is inferred that the primary response of the jet was an upward curvature of the jet centerline. A second inference is that the exterior region of the jet primarily responds to the z-component momentum since the pressure which agreed with the isotach intersection curve was invariant with respect to α when normalized by sin α (see p_{agree} column of Table 1). A rather detailed analysis allowed the location of the equivalent x-component momentum flux, z_m, to be determined. The curvature K of $z_m(x)$ was calculated from the pressure data. The curvature for the above case is shown in Figure 3 along with centerline pressure. The isobar data for α = 15 degrees, h/d = 1 and α = 60 degrees, h/d = z are shown in Figures 4 and 5 to demonstrate the first case for which a substantial widening occurred and the significant spreading effects at the largest angle investigated. The curvature and centerline pressure for these cases are shown in Figure 3b and 3c.

A characteristic set of isotach contours (plotted from the data of a single, vertically mounted, hot-wire probe) is presented in Figure 6. The localized distortion of the velocity field at the outer edge of the jet and near the plate is evident. Similar isotach behavior was

* contour of constant velocity

observed for the other cases investigated.

One of the most striking results of the present study was the physical displacement between the stagnation and the maximum pressure point of the centerline pressure distribution. The stagnation point was determined from the measurement of the velocity quite close to the surface (v_w) ($\Delta z/d \approx 0.03$) and the comparison of this value to that calculated as if the surface pressure represented the stagnation pressure. The experimental technique is demonstrated by Figure 7 and the results are shown in Figures 8, 9, and 10.

2.4. Interpretation

The relative lack of spreading effects and the strong curvature effects for shallow angle impingement is inferred from data characterized by Figure 2 and Table 1. The mechanistic description of the curvature is best effected by conservation of momentum principles in conjunction with the mean surface pressure data. The inference of the jet width from the surface pressure provides at least a conservative width measure; inertial effects may cause the velocity field to extend beyond the zero isobar. The lateral pressure distribution of Figure 6 demonstrates that such an effect occurs; this effect is increasingly pronounced with respect to increasing α. However, the region inside the zero isobar is considered to demonstrate the active width of the jet.

The deformation of the isotach contours, the isobar distributions and the vorticity considerations of 2.2 can be combined to interpret the basic mechanisms operative in this flow. Specifically, the isobar contours imply a strong flux of ω_x into the flow field near the edge of the jet where $\partial p/\partial y\big|_0$ term of (5) is large. Such vorticity is apparently retained in the region quite close to the surface; this is shown schematically as the near wall region in Figure 11. The large scale motion of the jet is initially constructed of ω_θ vorticity which is required to deform by the presence of the plate while maintaining the closed loops required by the solenoidal condition ($\nabla \cdot \nabla \times \underline{\omega} = 0$). This adjustment appears to result in the production of rather large scale (or distributed) ω_x from the initially azimuthal vorticity as demonstrated in Figure 11. Simultaneously with these effects, there is a significant stretching of the ω_y vorticity in the neighborhood of the centerline and near the plate surface. The ω_y vorticity of this region is stretched laterally by the large $\partial v/\partial y$ velocity gradient associated with the ω_x distribution in the near wall region. The strongly concentrated ω_y of this region is implied by the isotach contours which must pass between the plane of the plate and the undistorted isotaches in the central region of the jet (see Figure 6).

The velocity data from the stagnation point investigation in combination with equation (4) and the p(x, 0, 0) data allow the formation of a pertinent vorticity flux ratio. Specifically,

$$\frac{\text{vorticity flux through surface from 0 to x}}{\text{vorticity flux through area of height } \delta z \text{ at x}} = \frac{2[p(0,0,0) - p(x,0,0)]/\rho u^2(o)}{\overline{u}\,(x,0,\delta z)^2/u^2(o)} \qquad (6)$$

The ratio of equation (6) has been evaluated; the results are presented in Table 2.

Table 2. Ratio of ω_y vorticity flux through the plate to the voriticity flux through a small height at the x location of the maximum pressure. Uniform nozzle exit condition

α	h/d	x/d*	$\delta z/d$	$\{\frac{2}{\rho}[p(x,0,0)-p(0,0,0)]\}/\{u(x,0,\delta x)^2\}$
3	1	4.08	0.0328	14.54/46.2 = 0.315
9	1	2.13	---	27.4/49.9 = 0.55
15	1	1.25	---	46.2/63.6 = 0.73

These ratios show that a significant amount of $-\omega_y$ is added to the $+\omega_y$ vorticity near the plate for all cases. The vorticity so added increases rather strongly as α increases; this is reasonable based upon the observation of the centerline pressure relationship to the overall and local jet curvature effects. The data show that the $+\omega_y$ vorticity flux through δz increases in magnitude even as the $-\omega_y$ vorticity flux increases. This result is attributed to the importance of the production term due to stretching ($\omega_y \partial v/\partial y$). Consequently the production term is quite important in the description of the vorticity processes occurring in the flow. Since $\partial v/\partial y$ is related to the ω_x distribution, i.e., $v(x,y,\delta z) = [\partial v(x,y,0)/\partial z]\delta z = -\omega_z \delta z$, an analytical model would have to consider the simultaneous solution of the x and y components of vorticity.

3. ACOUSTIC EFFECTS

The following observations are speculations based upon the notion of vortex stretching as a generator of acoustic noise and the results presented in Section 2. The near wall region defined in Figure 11 is clearly the domain of the most important stretching effects. A principal result of [11] would be that the upper and central portion of the jet is essentially not distorted until its geometric projection is

sufficiently close to the plate surface. The strong ω_y of the near wall region is apparent from the isotachs; the importance of the ω_x distribution is perhaps less intuitive but it is also apparent in the isotachs and from the pressure data.

The location of the stagnation point near the upstream edge of the isobar distribution is a significant result. A consequence is that the vorticity downstream of the stagnation and near the plate is of the same sign as that of the approach flow. This contributes to the large spatial region of strong ω_y near the wall. In general, it would seem reasonable that the concentrated motions in the near wall region would result in substantial domains over which the velocity or vorticity fluctuations are correlated and that the presence of the strong mean vorticity would imply relatively strong vorticity fluctuations.

The vorticity in the neighborhood of the stagnation point is significantly different from that of a normally impinging jet. Figure 12 presents a schematic of the flow in the (x, 0, z) plane. The material element characterized as 1 is, by postulate, initially in a (time-mean) vortex loop with the element at 1a as required by the solenoidal condition. During the passage from B to C, the element will be required to become part of a different loop since it has changed the sign of its ω_y vorticity. It might join with the material element 2 although it also appears reasonable that 2 could remain in its original (time-mean) loop with 2a. This transfer will take place by the diffusive action of the viscous effects in the neighborhood of the stagnation point. Such a process likely occurs with large vorticity fluctuations. The neighborhood of the stagnation point would therefore seem to be a relatively important region as regards the acoustic emissions.

REFERENCES

1. Dorsch, R.G., Kreim, W.J., and Olsen, W.A., "Externally-Blown-Flap Noise," Paper 72-129, Jan. 1972, AIAA, New York, N.Y.
2. Putnam, T.W. and P.L. Lasagna "Externally Blow Flap Impingement Noise," AIAA Paper No. 72-664, 1972.
3. Haas, M. "Blown Flap Noise," MIT Report FTL 72-5, 1972.
4. Olsen, W., Miles, J., and Dorsch, R., "Noise Generated by Impingement of a Jet Upon a Large Flat Board," TN D-7075, 1972, NASA, Cleveland, Ohio.
5. Lighthill, M.J., "Introduction: Real and Ideal Fluids," Laminar Bounadry Layers, L. Rosehead, Ed., Oxford University Press, 1963.
6. Powell, A., "Theory of Vortex Sound," Jour. of the Acoutical Society of America, 36, 1, 177-195, January 1964.
7. Curle, N., "The Influence of Solid Boundaries upon Aerodynamic Sound," Proc. Roy. Soc. A 231, 505-514.

8. Ffowcs, Williams J.E. and Hawkings, D.L., "Sound Generation by Turbulence and Surfaces in Arbitrary Motion.

9. Lighthill, M.J., "On Sound Generated Aerodynamically I. General Theory," Proc. of the Roy. Soc. of London, Ser. A, Vol. 211. No. 1107 Mar. 20, 1952, pp. 564-587.

10. Lighthill, M.J., "On Sound Generate Aerodynamically. II. Turbulence as a Source of Sound," Proc. of the Roy. Soc. of London, Ser. A, Vol. 222, No. 1148, February 23, 1954, pp. 1-32.

11. Foss, J.F. and S.J. Kleis, "The Oblique Impingement of an Axisymmetric Jet," Second Annual Report to NASA, NGR-23-004-068, Michigan State University, 1972.

12. Donaldson, C. DuP. and R. Snedecker, "A Study of Free Jet Impingement. Part 1. Mean Properties of Free and Impinging Jets," Jour. Fluid Mech. vol. 45, p. 2, 1971.

13. Donaldson, C. DuP., R.S. Snedecker and D.P. Margolis, "A Study of Free Jet Impingement. Part 2. Free Jet Turbulent Structure and Impingement Heat Transfer," Jour. Fluid Mech. vol. 45, p. 3 1971.

Table 1. Summary of percent widths, distance to maximum pressure and isobar which aligns with free isotach intersection.

		Width of 0.1 free isotach intersection contour as a percentage of the zero isobar width recorded at the x-location of the maximum pressure		x/d distance from x=0 to p max		P_{agree_2} $\frac{}{\rho u(0)^2 \sin \alpha}$ all x 10^{-2}		x/d distance from x=0 to 0.1 free isotach intersection	
α	b/d	u	fd	u	fd	u	fd	u	fd
3	0.5625	--	74	--	0.7	--	0.57	--	0.321
	0.667	--	80	--	2.3	--	0.31	--	1.003
	0.75	0.75	80	4.5	2.9	0.35	0.266	1.663	1.544
	1	0.68	78	5.9	5.7	0.38	0.266	3.543	3.176
6	0.75	0.69	76	1.9	2.1	0.36	0.30	1.16	1.18
	1	0.75	71	4.7	4.2	0.29	0.30	2.5	2.324
	1.5	0.64	68	6.4	7	0.20	0.22	5.178	4.737
9	1	0.64	71	3.2	3.3	0.38	0.27	1.91	1.81
	1.5	0.65	70	5.7	6.2	0.25	0.22	3.715	3.979
	2	--	66	--	7.5	--	0.18	--	5.619
12	1	--	--	--	--	--	--	--	--
	1.5	0.58	65	5	5.1	0.28	0.224	3.202	3.029
	2	--	65	--	7.2	--	0.22	--	4.59
15	1	0.46	--	2	--	1.0	--	1.247	--
	1.5	--	--	--	--	--	--	--	--
	2	--	61	--	6	--	0.24	4.06	3.895
30	2	0.3	--	3.4	--	0.65	--	1.978	--
	3	0.36	--	5.2	--	0.61	--	3.429	--
60	2	0.25	--	1.9	--	0.92	--	0.37	--

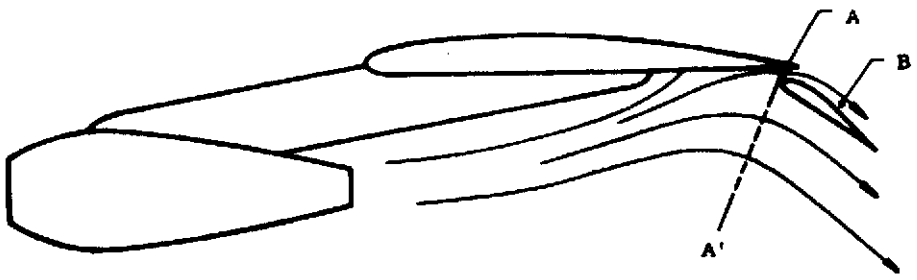

Figure 1a. Externally blown flap STOL aircraft configuration.

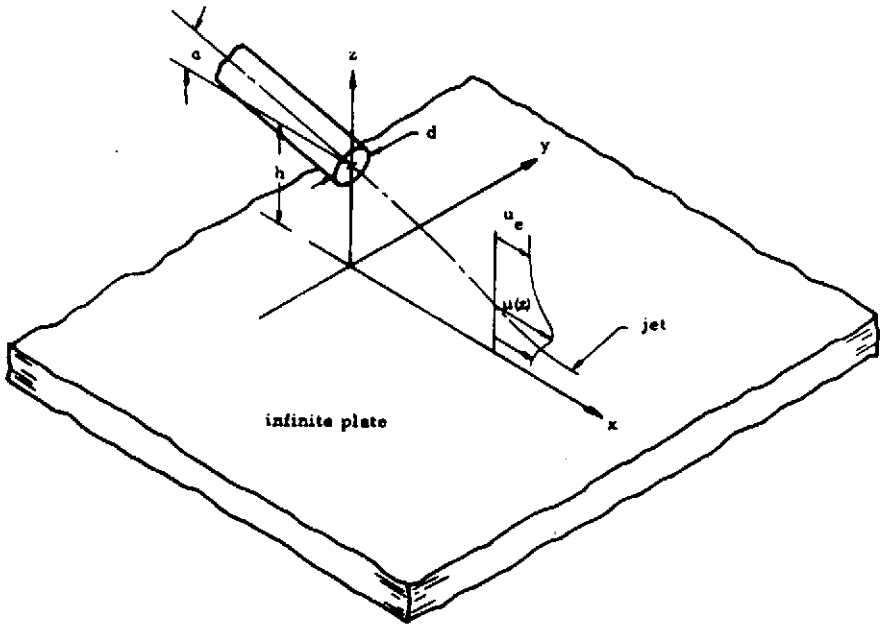

Figure 1b. The round-jet/plane-wall flow field, coordinate system and nomenclature.

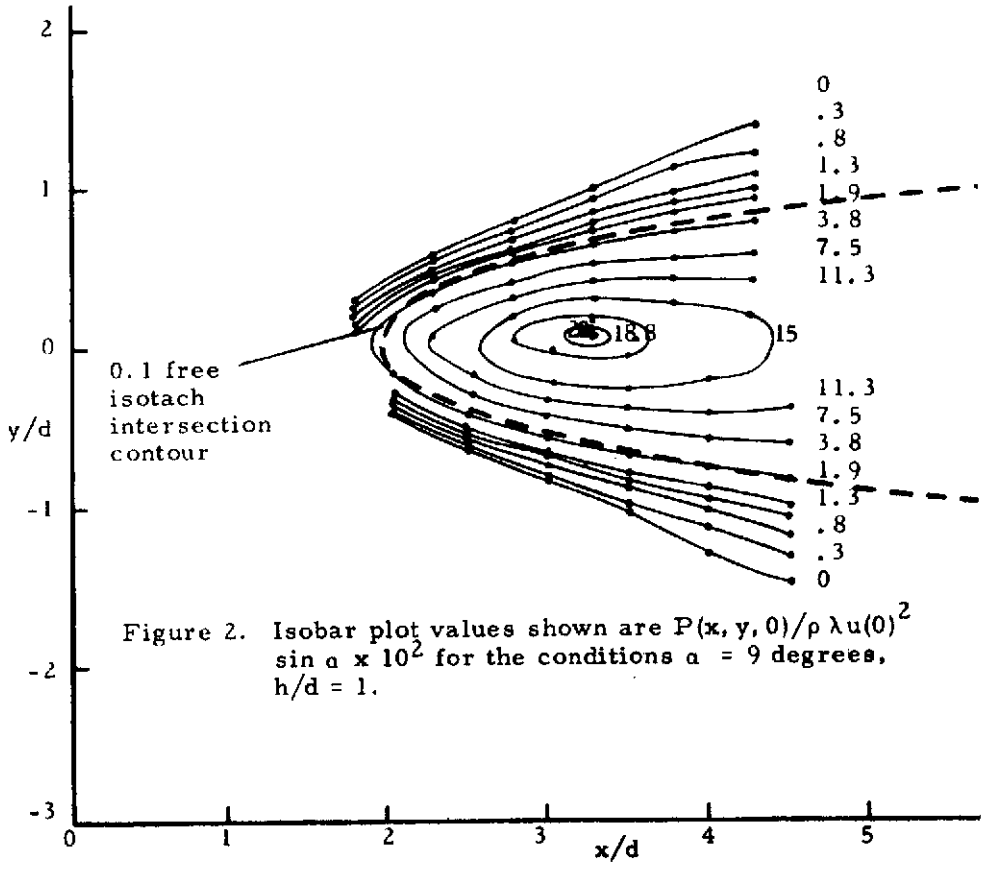

Figure 2. Isobar plot values shown are $P(x, y, 0)/\rho \lambda u(0)^2$ sin α x 10^2 for the conditions α = 9 degrees, h/d = 1.

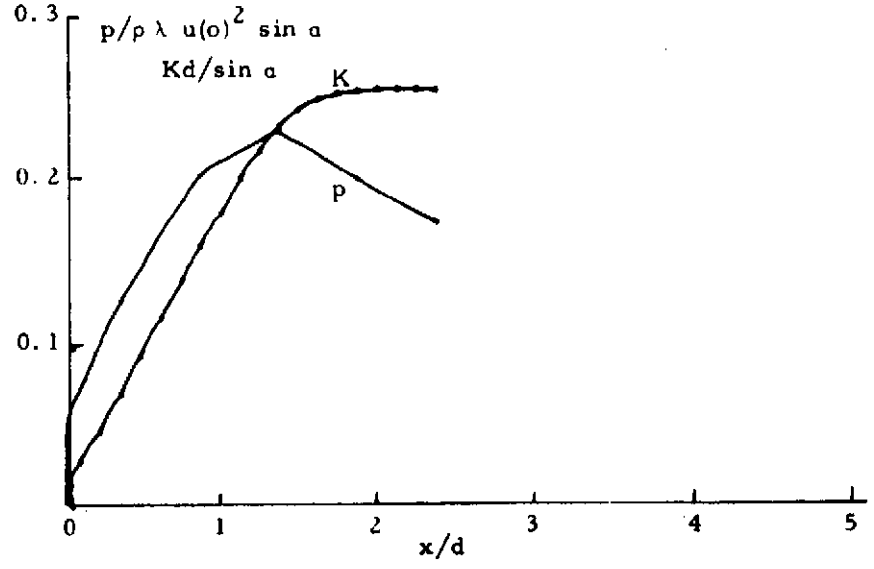

Figure 3a.

Normalized centerline pressure $p/\rho \lambda u(o)^2$ sin α and the normalized curvature of the jet's momentum flux centerline Kd/sin α . The x/d = 0 origin for each h/d value represents the intersection point of the 0.1 free isotach.
α = 9 degrees h/d = 1

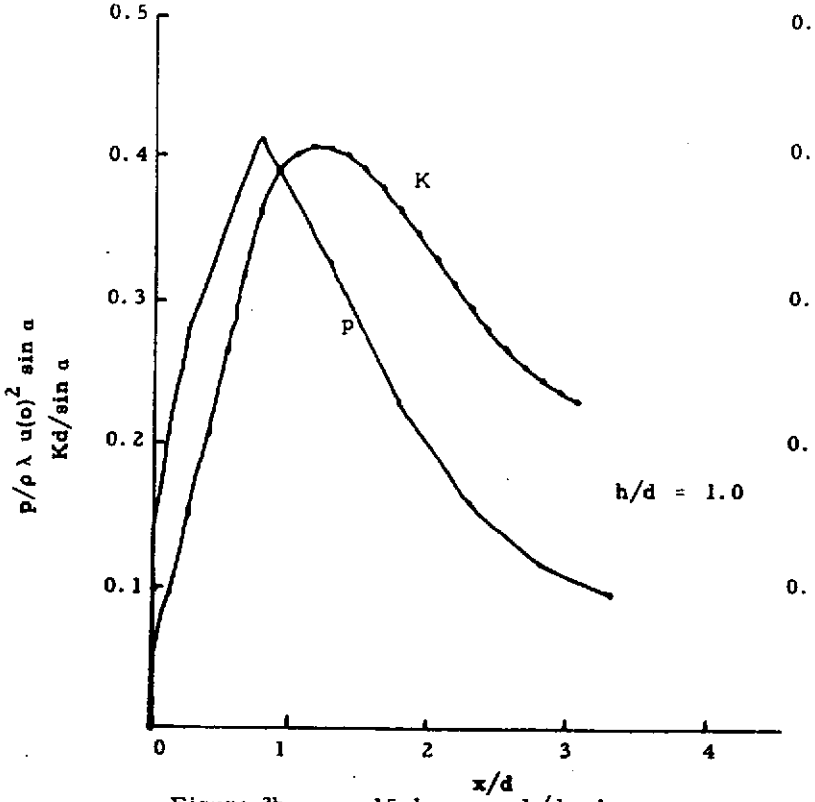

Figure 3b. α = 15 degrees, h/d = 1.

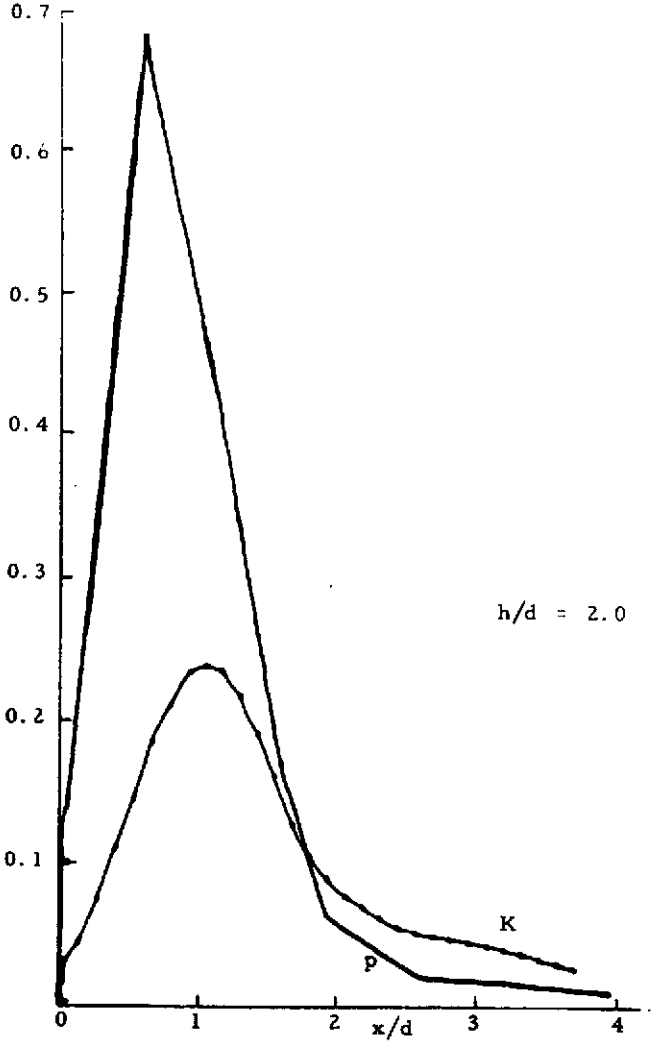

Figure 3c. α = 60 degrees, h/d = 2.

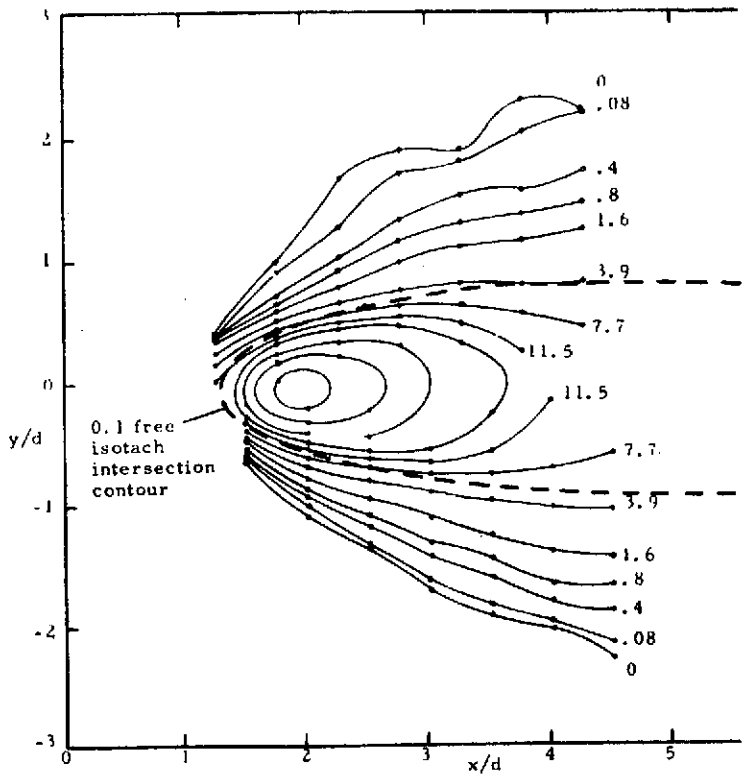

Figure 4. Isobar plot values shown are $p(x, y, 0)/\rho \lambda u(0)^2 \sin \alpha \times 10^2$ for the conditions $\alpha = 15$ degrees, $h/d = 1$.

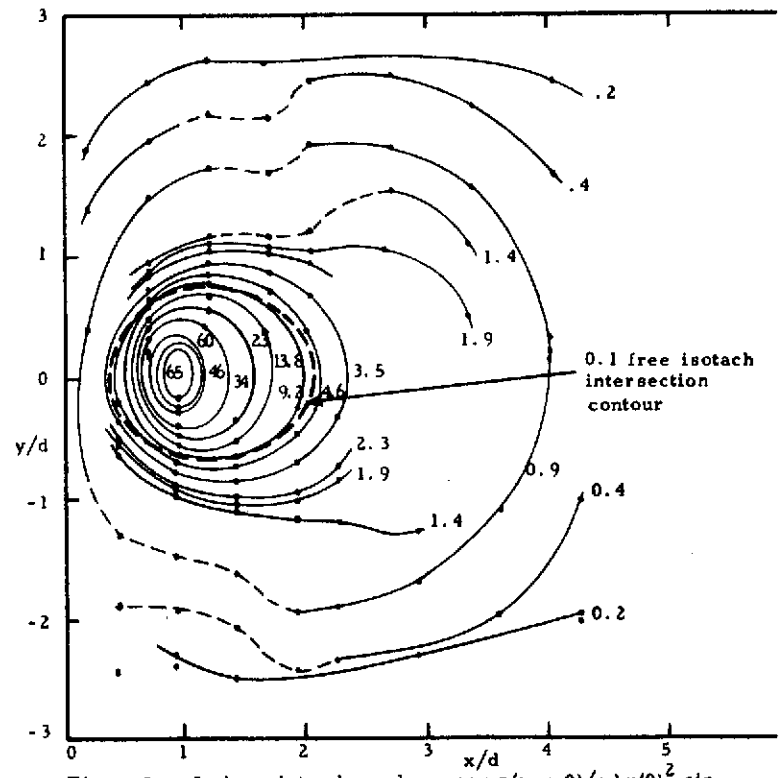

Figure 5. Isobar plot values shown are $p(x, y, 0)/\rho \lambda u(0)^2 \sin \alpha \times 10^2$ for the conditions $\alpha = 60$ degrees, $h/d = 1$.

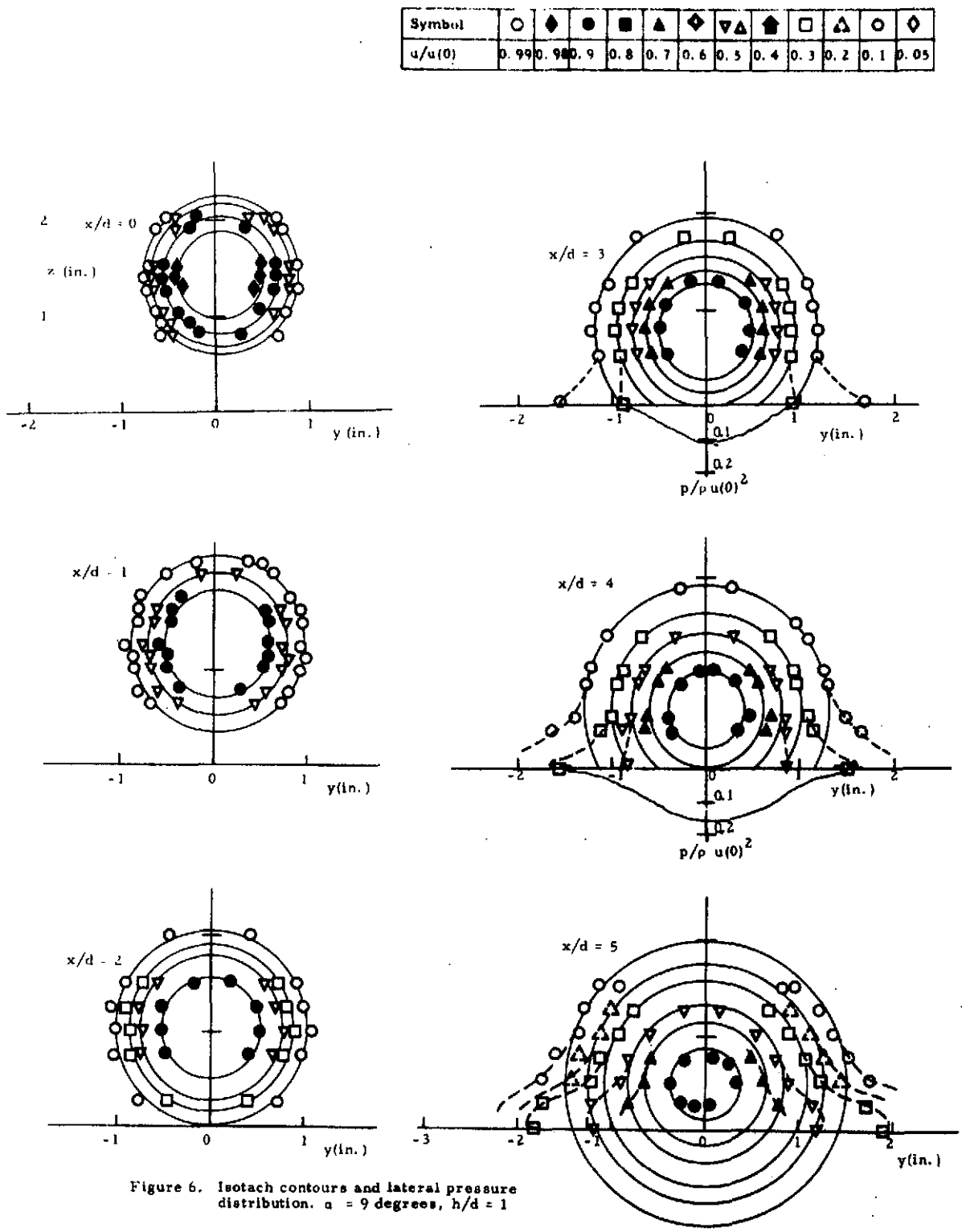

Figure 6. Isotach contours and lateral pressure distribution. α = 9 degrees, h/d = 1

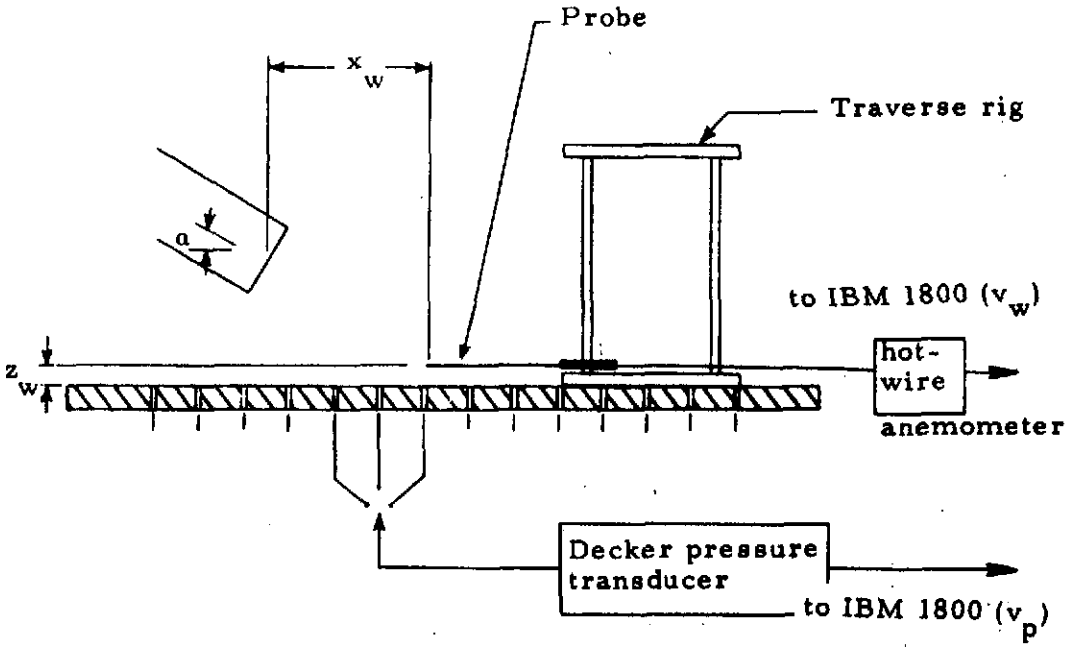

Note: For the comparison of the hot-wire and pressure data, v_w was shifted in x by an amount $v_w(x, z) = v_w(x+\Delta x, 0)$ where $\Delta x = \Delta z/\tan(\alpha + \beta)$.

Figure 7. Experimental technique for the acquisition of the velocity and surface static pressure data.

$$v_p(x, 0, 0) = \frac{2}{\rho}[p(x, 0, 0) - p_{atm}]^{1/2}$$

$v_w(x, 0, 0)$ = v measured at $z/d = 0.0328$ and shifted by $\Delta x = \Delta z/\tan(\alpha + \beta)$ (β = spread angle of 0.1 free isotach)

Solid curve shows additional shift to indicate the stagnation point.

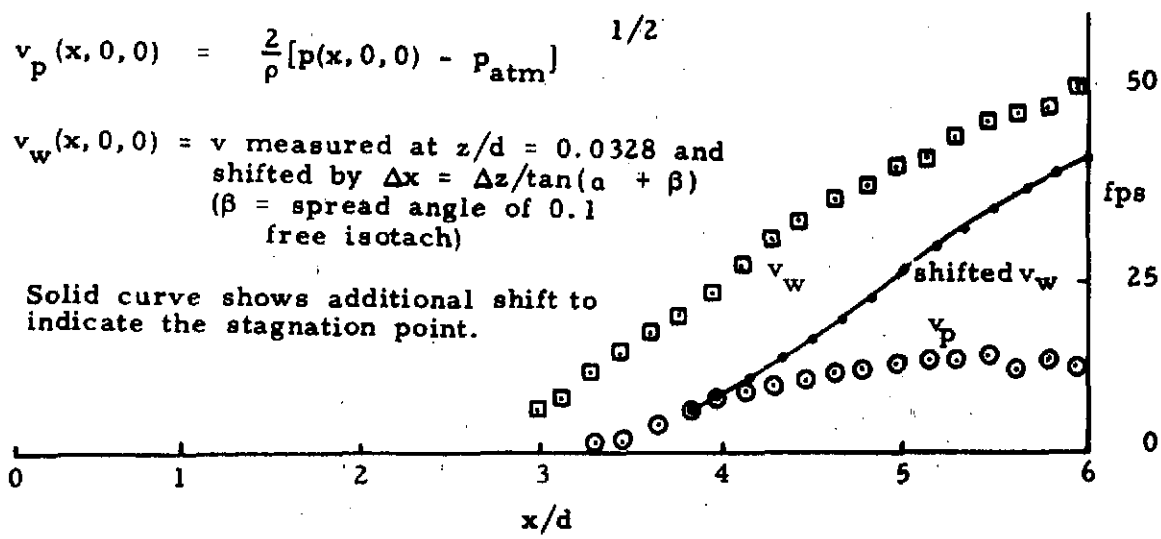

Figure 8.
Measured, v_w, and equivalent stagnation streamline velocities (as inferred from the surface pressure), v_p, to determine the stagnation point for the conditions α = 3 degrees, h/d = 1, uniform.

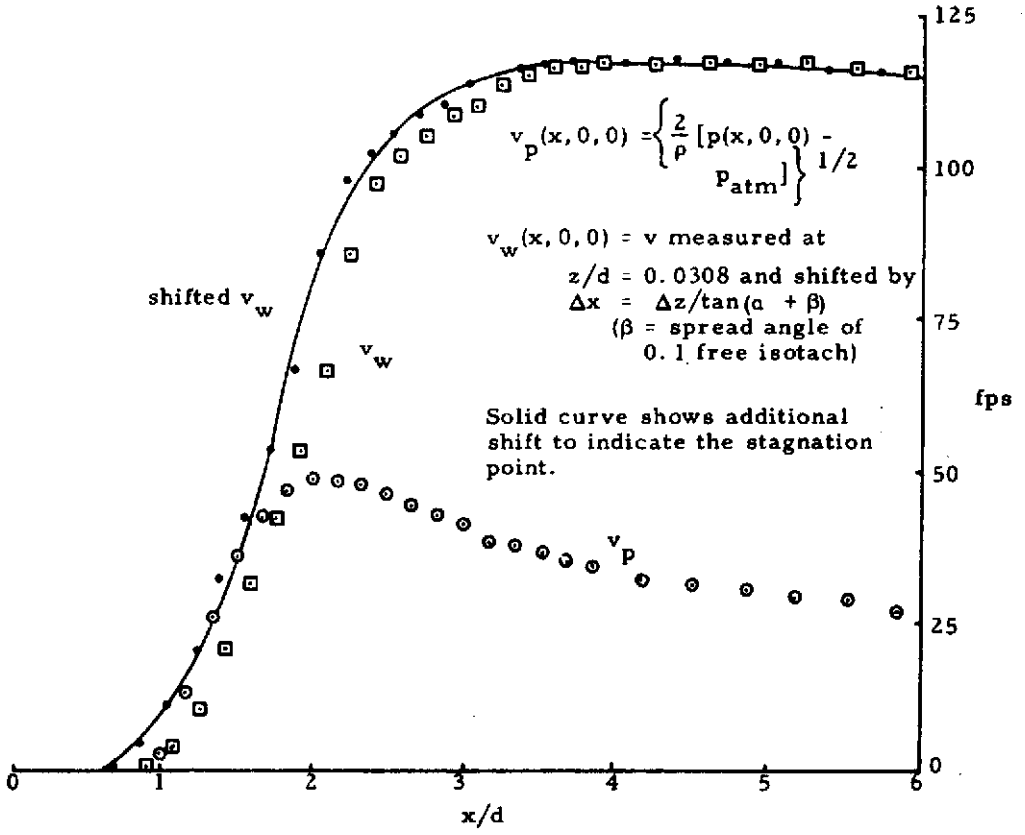

Figure 9. Measured, v_w, and equivalent stagnation streamline velocities (as inferred from the surface pressure), v_p, to determine the stagnation point for the conditions α = 15 degrees, h/d = 1, uniform.

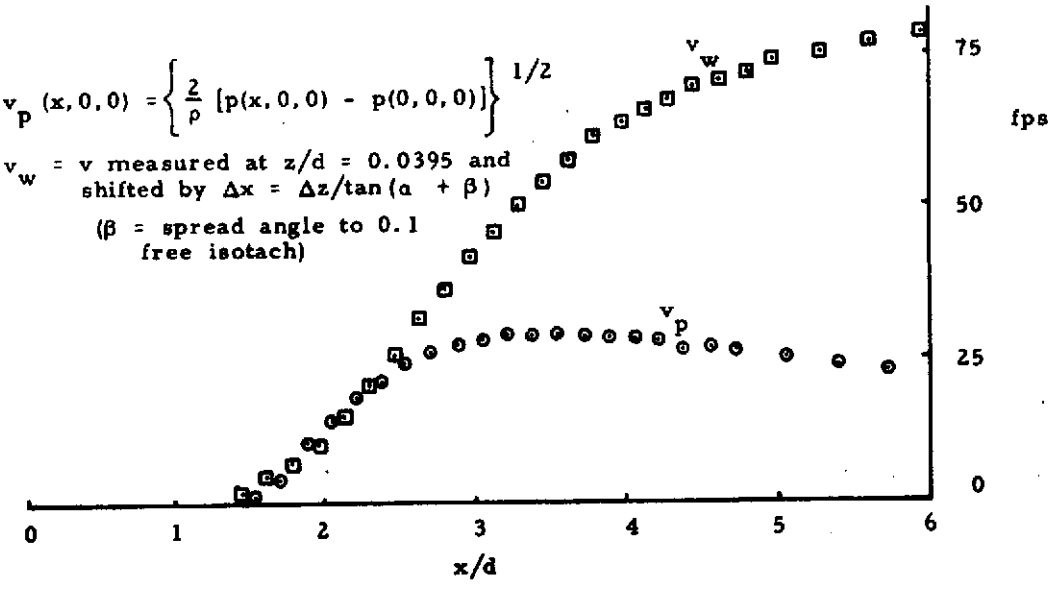

Figure 10. Measured, v_w, and equivalent stagnation streamline velocities (as inferred from the surface pressure), v_p, to determine the stagnation point for the conditions α = 9 degrees, h/d = 1, uniform.

Axisymmetric region, azimuthal vorticity of the approaching jet flow.

Buffer region, Streamwise vorticity production from reorientation of the azimuthal vorticity field ($\omega_0 \partial u/\partial \theta$).

Near wall region, streamwise vorticity from flux at wall ($\nu \partial \omega_x/\partial z$) and vortex stretching ($\omega_y \partial u/\partial y$). Spatial extent is exaggerated.

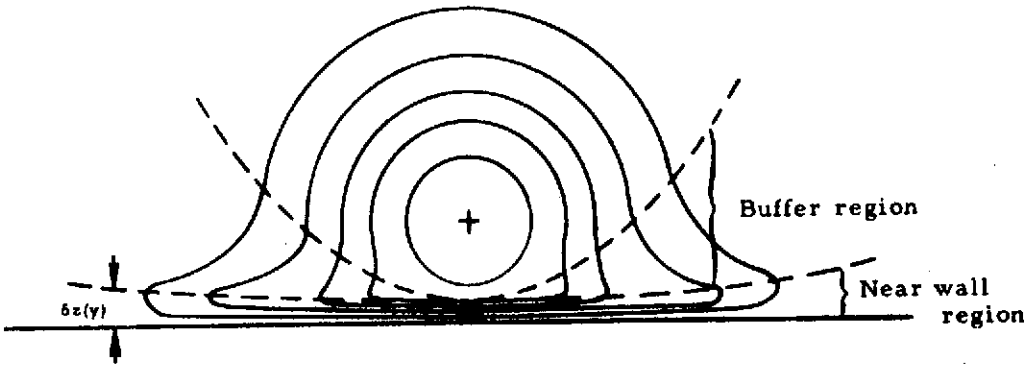

Figure 11. Schematic representation of general isotach distribution showing the axisymmetric region in the undisturbed flow, the buffer region and the near wall region.

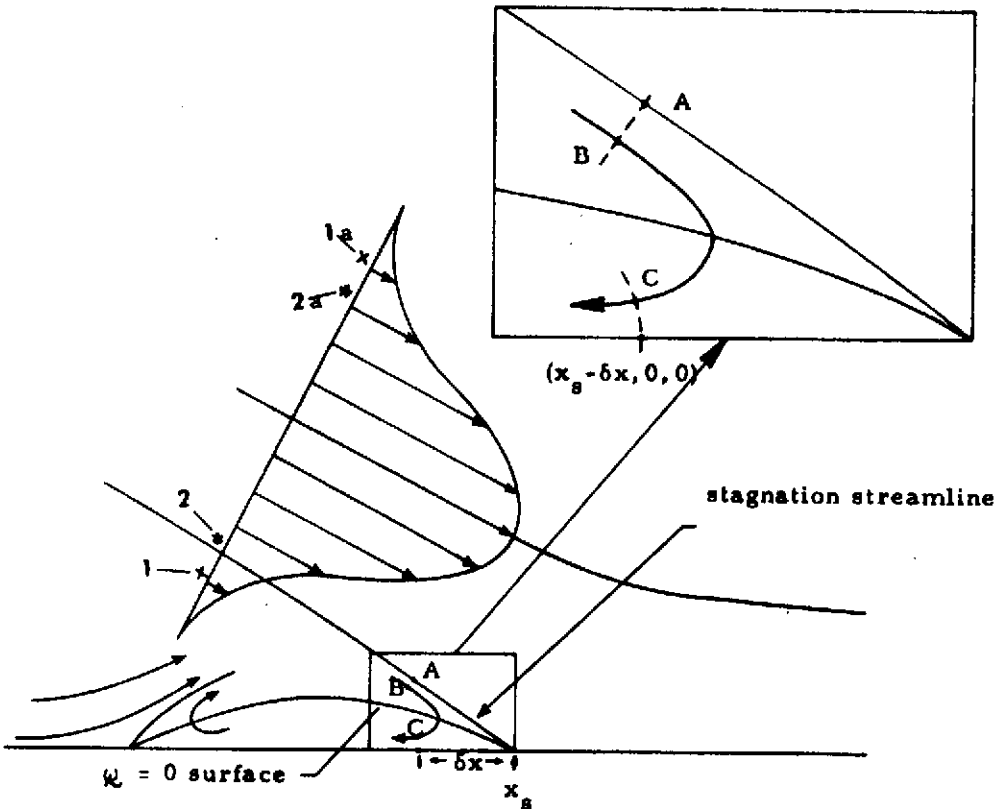

Figure 12. Physical characteristics of oblique jet impingement.

APPENDIX C

Flow Field Measurements in the Impingement Region of an Oblique Jet

J. F. Foss, Associate Professor
Dept. of Mech. Engr. and Div. of Engr. Research
Michigan State University, East Lansing, Michigan 48824

ABSTRACT

Reduction of the acoustic noise generation in the impact region of the under-wing externally blown flap configuration is an important factor in its acceptance as a propulsion technique for STOL aircraft. Three-dimensional traverses to document the mean velocity and Reynolds stress distributions in the noise producing region of an oblique (45 degrees) axisymmetric jet impingement (L/D = 7) flow field have been made. The stretching and reorientation of the approach vorticity and the strong vorticity production by the surface pressure field which have been shown to control the mechanics of the shallow angle impingement flow will be examined by vorticity measurements. These measurements can be combined with vorticity-acoustics considerations to interpret the noise producing characteristics of this flow.

APPENDIX D

The Influence of the Exit Plane Turbulence Conditions on the Noise Producing Region of an Axisymmetric Jet

Stanley J. Kleis* and John F. Foss
Division of Engineering Research
Michigan State University
East Lansing, Michigan 48824

ABSTRACT

The effect of the exit plane conditions on the initial region ($0 \leq x/D \leq 10$) of an axisymmetric jet has been systematically investigated. An essentially top-hat mean velocity profile and a homogeneous turbulence structure were maintained at the exit plane for eight distinct scale and intensity conditions. Mass and momentum flux values are "independent" of the exit turbulence structure for the range investigated; however, a significant ($\simeq$ 25 percent) increase in the latter implies a pronounced static pressure decrement inside the jet. Details of the velocity profile and turbulence structure are influenced by the exit plane conditions. The three radial-axial components of the Reynolds stress tensor have been conditionally sampled (eight exit conditions, $0.5 \leq x/D \leq 10$) and are analyzed to show the initial condition effects.

*Presently Assistant Professor at the University of Houston, Houston, Texas.